

## Structure of $^{118}\text{Sb}$ nucleus

J. Gulyás, T. Fényes, M. Fayez F. M. Hassan,\* and Zs. Dombrádi

*Institute of Nuclear Research of the Hungarian Academy of Sciences, H-4001 Debrecen, Hungary*

J. Kumpulainen and R. Julin

*University of Jyväskylä, Department of Physics, SF-40351 Jyväskylä 10, Finland*

(Received 17 March 1992)

$\gamma$ ,  $\gamma\gamma$ -coincidence, internal conversion electron, and  $\gamma$ -ray angular distribution spectra of the  $^{118}\text{Sn}(p,n\gamma)^{118}\text{Sb}$  reaction were measured at different bombarding proton energies between 5.5 and 7.5 MeV.  $\gamma$ ,  $\gamma\gamma$ -coincidence, and internal conversion electron spectra of the  $^{115}\text{In}(\alpha,n\gamma)^{118}\text{Sb}$  reaction were also measured at  $E_\alpha = 14.5$  MeV. Ge(HP), Ge(Li), Ge(LEPS)  $\gamma$ -ray detectors, as well as a superconducting magnetic lens electron spectrometer [with Si(Li) detectors], were used in the experiments. About 210 (including  $\sim 130$  new)  $\gamma$  rays have been assigned to  $^{118}\text{Sb}$ . The deduced  $^{118}\text{Sb}$  level scheme contains more than 70 new levels. On the basis of the internal conversion coefficients, Hauser-Feshbach analysis of  $(p,n)$  reaction cross sections,  $\gamma$ -ray angular distributions, and other arguments spin and parity values have been determined. The “parabolic rule” prediction of the energy splitting of different proton-neutron multiplets enabled the identification of many proton-neutron multiplet states. The energy spectrum and electromagnetic properties have been calculated in the framework of the interacting boson-fermion-fermion-odd-odd truncated quadrupole phonon model, and reasonably good agreement has been obtained between experimental and theoretical results.

PACS number(s): 23.20.Lv, 23.20.En, 27.60.+j, 25.40.Kv

### I. INTRODUCTION

The low-lying levels of the  $^{118}\text{Sb}$  nucleus were studied mainly from  $(p,n\gamma)$  and other light-particle reactions by Chaffe *et al.* [1–3]. A negative-parity, high-spin band was observed in  $^{118}\text{Sb}$  by Vajda *et al.* [4] from (heavy ion,  $xn$ ) reactions. The electron capture of  $^{118}\text{Te}$  feeds only the ground state of  $^{118}\text{Sb}$  [5]. Electromagnetic moments are known for the ground and four isomeric states of  $^{118}\text{Sb}$  [6–12].

According to the compilation of Tamura, Miyano, and Ohya [13], about 56 levels are known in  $^{118}\text{Sb}$  below 3000 keV excitation energy, but unambiguous spin-parity values have been determined only for the  $1^+$  ground and  $8_1^-$  isomeric states. The excited levels of  $^{118}\text{Sb}$  were not studied up to now from the  $^{115}\text{In}(\alpha,n\gamma)^{118}\text{Sb}$  reaction. A theoretical description of the structure of  $^{118}\text{Sb}$  nucleus is missing.

The aim of the present work was a complex  $\gamma$  and electron spectroscopic study of the excited levels of  $^{118}\text{Sb}$ , with special emphasis on the determination of spin-parity values. We have measured  $\gamma$ ,  $\gamma\gamma$ -coincidence, and conversion electron spectra of the  $(p,n\gamma)$  and  $(\alpha,n\gamma)$  reactions at different bombarding particle energies. The angular distribution of  $\gamma$  rays has also been studied from the  $(p,n\gamma)$  reaction. The energy splitting of different proton-neutron multiplet states has been calculated as a function of spin. These “parabolic rule” calculations proved to be useful for the identification of proton-

neutron multiplet states. In the framework of the interacting boson-fermion-fermion-odd-odd truncated quadrupole phonon model (IBFFM-OTQM), we calculated the  $^{118}\text{Sb}$  energy spectrum, electromagnetic moments, and  $\gamma$ -ray branching ratios.

### II. EXPERIMENTAL TECHNIQUES

We have used 0.3–2.5-mg/cm<sup>2</sup>-thick, self-supporting  $^{118}\text{Sn}$  and  $^{115}\text{In}$  targets in the  $(p,n\gamma)$  and  $(\alpha,n\gamma)$  experiments, respectively. For reliable identification of  $\gamma$  rays, we have also studied the  $^{116,119,120}\text{Sn}+p$  and  $^{113}\text{In}+\alpha$  reactions with  $\gamma$ -spectroscopic methods. The final identification was made on the basis of  $\gamma\gamma$ -coincidence measurements. The  $^{116}\text{Sn}$ ,  $^{118}\text{Sn}$ ,  $^{119}\text{Sn}$ , and  $^{120}\text{Sn}$  as well as the  $^{113}\text{In}$  and  $^{115}\text{In}$  target materials were isotopically enriched up to 97.8%, 98.7%, 86.7%, 99.6%, 93.1%, and 99.99%, respectively. The targets were prepared by the evaporation technique.

#### A. The $(p,n\gamma)$ reaction

The  $Q$  value of the  $^{118}\text{Sn}(p,n)^{118}\text{Sb}$  reaction is  $-4.44$  MeV [14]. The targets were bombarded with 5.5–7.5 MeV energy and 10–1000-nA-intensity proton beams of the Debrecen 103-cm Isochronous Cyclotron.

The  $\gamma$ -ray spectra were measured with a 25% relative efficiency coaxial Ge(HP) detector and a  $2000 \times 13\text{-mm}^3$  planar Ge(HP) low energy photon spectrometer (LEPS), placed at  $90^\circ$  to the beam direction for energy determination and at  $125^\circ$  for intensity measurements. The energy resolutions [full width at half maximum (FWHM)] of the coaxial and planar detectors were 2 keV (at 1332 keV) and 0.8 keV (at 122 keV), respectively. For energy and

\*Present address: Atomic Energy Authority, Experimental Nuclear Research Centre, 13758 Cairo, Egypt.

efficiency calibration of the spectrometers,  $^{133}\text{Ba}$  and  $^{152}\text{Eu}$  radioactive sources were used. The energies of the strong 115.4(1)-, 128.4(4)-, and 324.2(4)-keV  $^{118}\text{Sb}$  [13] and 1229.64(3)-keV  $^{118}\text{Sn}$  [13] internal calibration lines have been well reproduced.

The  $\gamma\gamma$ -coincidence spectra were measured at 7.5 MeV bombarding proton energy with two coaxial Ge(Li) detectors (of 70 cm<sup>3</sup> active volume each) and at 5.7 MeV proton energy with the 25% coaxial Ge(HP) and LEPS detectors mentioned above. The  $\gamma\gamma$ -coincidence data were recorded in an event-by-event mode on magnetic tapes with a fixed  $\tau=100$  ns resolving time and were sorted off line. After creating the symmetrized two-dimensional coincidence matrices, a standard gating procedure was used to obtain coincidence spectra. Altogether, about  $1.5 \times 10^7$  coincidence events were acquired.

The internal conversion electron spectra were measured with a superconducting magnetic lens plus Si(Li) spectrometer [15]. The energy resolution and transmission of the spectrometer were  $\sim 2.7$  keV FWHM (at 946 keV) and 10% [for two Si(Li) detectors], respectively. The background from backscattered electrons was reduced with a swept energy window in the spectrum of the Si(Li) detector. Further background reduction was achieved with twisted paddle-wheel-shaped antipositron baffles. For the calibration of the spectrometer,  $^{133}\text{Ba}$  and  $^{152}\text{Eu}$  sources were used.

We estimated the effect of angular distribution of electrons on the measured internal conversion coefficients by the use of the available  $\gamma$ -ray angular distribution coefficients, solid-angle correction factors [15] (for the electron spectrometer), and normalized directional particle parameters. The estimation showed that this effect was usually much less than the statistical uncertainties of the measured internal conversion coefficients.

The  $\gamma$ -ray angular distribution were measured at 5.6 MeV bombarding proton energy at different angles with respect to the beam direction from 90° to 145°, in 5° steps. The solid-angle correction factors for the detector were  $Q_2=0.975$  and  $Q_4=0.915$ . For normalization of the  $\gamma$ -ray intensities, we used a germanium monitor detector at fixed position.

The theoretical angular distributions for different spin combinations were fitted to the experimental data in a least-squares procedure using the computer code ANDIST [16]. The  $\alpha_2$  and  $\alpha_4$  attenuation coefficients were calculated with the CINDY [17] program. If the level was fed by  $\gamma$  ray(s), the reorientation effect was also taken into account. The optical potential parameters used in the calculations are given in Sec. V.

### B. The $(\alpha, n\gamma)$ reaction

$\alpha$  beams of the Jyväskylä 90-cm and Debrecen 103-cm Isochronous Cyclotrons were used in the experiments. The energy of  $\alpha$  particles was 14.5 MeV. This is several MeV higher than the threshold of the  $(\alpha, n)$  reaction on  $^{115}\text{In}$ , but is slightly below the  $(\alpha, 2n)$  reaction threshold. The  $\alpha$ -beam intensity was 5–10 and 300–400 nA in the  $\gamma$ - and electron-spectroscopic measurements, respectively.

A 20% relative efficiency and  $\sim 2$  keV energy resolution (at 1332 keV) Ge(HP) detector was used for the determination of the energy and relative intensity of  $\gamma$  rays. It was placed at 90° (with respect to the beam direction) for energy and at 125° for the intensity measurements.

The  $\gamma\gamma$ -coincidence measurements were performed also at 14.5 MeV bombarding  $\alpha$ -particle energy with 15% Ge(HP), 20% Ge(HP), and a  $200 \times 7$  mm<sup>3</sup> Ge(HP, LEPS) detectors, which were placed at  $\sim 55^\circ$ ,  $\sim 125^\circ$ , and  $\sim 235^\circ$  relative to the beam direction. The fixed coincidence resolving time of  $\tau=70$  ns was set in a fast overlap coincidence system. The data were recorded in an event-by-event mode on magnetic tapes and were sorted off line using the DATAP [18] data-acquisition and sorting system. Approximately  $2.7 \times 10^7$  coincidence events were acquired. The good statistics enabled determination of energies and relative intensities of  $\gamma$  rays even in cases when they were unresolved in singles spectra.

The internal conversion electron spectra were studied with a superconducting magnetic lens spectrometer [supplied with Si(Li) detectors], in a similar way as in the case of the  $(p, n\gamma)$  reaction. The theoretical internal conversion coefficient of the 324.28-keV  $M1$  transition (with very small  $E2$  admixture) was used for normalization of experimental  $\gamma$ -ray and electron intensities.

The processing of the spectra was carried out with the FORGAMMA [19] spectrum-analysis program in both reaction studies.

## III. EXPERIMENTAL RESULTS

Typical  $\gamma$ -ray and internal conversion electron spectra are shown in Fig. 1. The measurements of  $\gamma$ -ray spectra of the  $^{116,118,119,120}\text{Sn}+p$  and  $^{113,115}\text{In}+\alpha$  reactions, as well as the study of the radioactive decay of the reaction products, enabled unambiguous identification of many  $^{118}\text{Sb}$   $\gamma$  rays. In some cases, when the  $\gamma$  rays were weak and unresolved in singles spectra, the identification, as well as the determination of energies and intensities, were made on the basis of  $\gamma\gamma$ -coincidence measurements.

From the intensity ratio of  $K$  and  $L$  conversion electron lines  $M1(+E2)$  multipolarity can be deduced for the 324.3-keV  $^{118}\text{Sb}$  transition. The  $E2/M1$  mixing ratio for this line is  $-0.09(17)$  from  $\gamma$ -ray angular distribution measurements. As the difference of the theoretical  $\alpha_K$  conversion coefficients for  $M1$  and  $E2$  multiplicities is very small for the 324.3-keV transition, this line could be used to normalize experimental data to the theoretical ones [20]. With this normalization the conversion coefficients of the 115.4-keV,  $M1$   $^{118}\text{Sb}$  transition [13] was fairly well reproduced. The  $\alpha_K$  internal conversion coefficients (ICC's) of  $^{118}\text{Sb}$  transitions are shown in Fig. 2.

Typical  $\gamma\gamma$ -coincidence spectra are shown in Fig. 3.

The energies, relative intensities, and  $\gamma\gamma$ -coincidence relations of  $^{118}\text{Sb}$   $\gamma$  rays, as well as the derived and formerly known multiplicities of transitions, are summarized in Tables I and II for  $(p, n\gamma)$  and  $(\alpha, n\gamma)$  reactions, respectively.

The reduced  $\chi^2$  fits of the theoretical angular distribu-

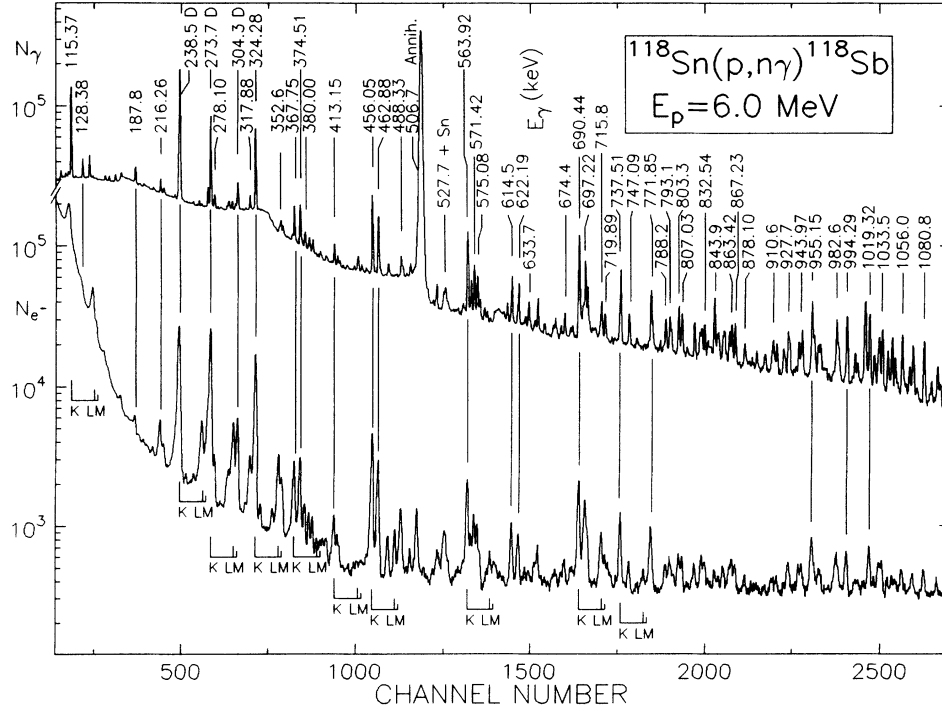


FIG. 1. Typical  $\gamma$ -ray and internal conversion electron spectra.  $\gamma$ -ray energies are given only for the strongest  $^{118}\text{Sb}$  transitions.  $K, L, M$  denote the corresponding conversion electron lines.  $D$  means doublet.

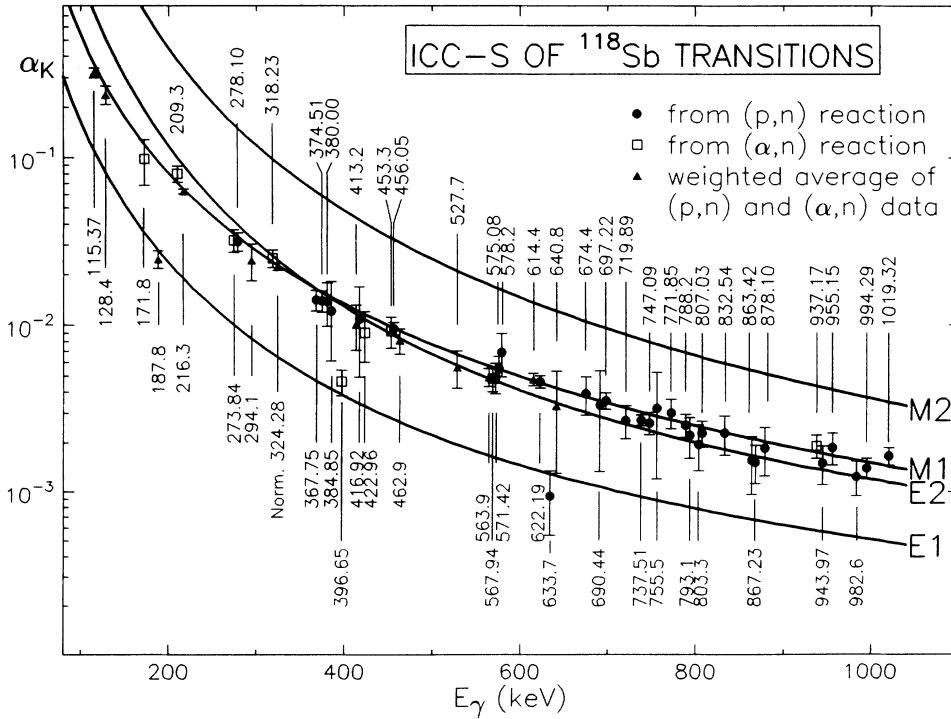


FIG. 2. Theoretical [20] (solid lines) and experimental (dots with error bars)  $\alpha_K$  internal conversion coefficients of  $^{118}\text{Sb}$  transitions as a function of  $\gamma$ -ray energy ( $E_\gamma$ ).

TABLE I. Energies, relative intensities, internal conversion coefficients, and multiplicities of  $\gamma$  rays observed in the  $^{118}\text{Sn}(p,n\gamma)^{118}\text{Sb}$  reaction at  $E_p=6.0$  MeV. [*S* and *S'* denote placement into the level schemes of Figs. 5 and 6, respectively; *N* denotes a new  $\gamma$  ray. The asterisk means that multiplicity has been determined also from the  $(\alpha,n\gamma)$  reaction in this work (see Table II). Coincident  $\gamma$  rays were detected at  $E_p=7.5$  MeV.]

$E_\gamma$ (keV)	$I_\gamma$ (relative)		ICC measurement		Former results	Coincident $\gamma$ rays (keV)								
			$10^3\alpha_k$	$\gamma$ multipol.										
31.2(2) [10]		<i>S</i>												
50.82(5)	90(10)	<i>S</i>			<i>E2</i> [7]									
103.65(3)	46(2)	<i>S</i>			<i>E1</i> [10]	115	128	413						
109.0(3)	< 17	<i>N</i>												
112.22(3)	28(1)	<i>S</i>				115	274	305	324	463				
115.37(3)	927(20)	<i>S</i>	340(30)	<i>M1</i>	<i>M1</i> [10]	104	112	128	154	158	237	318		
					*	375	385	456	463	575	697	774		
						833	994							
128.38(3)	85(2)	<i>S</i>	210(80)	<i>M1(+E2)</i>	*	104	115	172	188	208	239	284		
						595								
153.8(2)	17(1)	<i>S</i>				115	237	353						
158.2(1)	16(1)	<i>S</i>				115								
171.7(2)	20(5)	<i>S</i>			*	104	115	128	188	239	595			
187.8(1)	53(3)	<i>S</i>	23.4(40)	<i>E1</i>		128	368	564	716					
208.1(1)	12(3)	<i>S,N</i>				128	239							
216.26(3)	38(2)	<i>S</i>	62.6(20)	<i>M1,E2</i>	*	273.6	324							
232.8(1)	7(1)	<i>S</i>				273.7								
237.34(5)	200(50)	<i>S</i>				115	154	385	621	641	692			
238.54(3)	900(200)	<i>S</i>				128	172	208	368	413	564	595		
						716	747	803	847	855	944	983		
						1025								
273.6(1)	219(30)	<i>S</i>				112	216	298	305	417	539	674		
						720	772	793	807	829	844	928		
273.7(1)	277(40)	<i>S</i>			*	233	294	304	528	614	867	955		
278.10(3)	33(2)	<i>S'</i>	31.5(40)	<i>M1(+E2)</i>		575	690							
284.4(1)	9(5)	<i>S,N</i>				128	239							
294.1(1)	22(1)	<i>S</i>	22.4(80)	<i>M1</i>	*	273.7								
297.92(3)	19(1)	<i>S</i>				273.6	318	324						
304.3(3)	48(5)	<i>S,N</i>				273.7								
304.7(1)	25(5)	<i>S</i>				112	273.6	324	488	634				
317.88(6)	36(1)	<i>S</i>				115	298	456	571	622				
324.28(3)	417(5)	<i>S</i>	22.2(10)	<i>M1(+E2)</i>	*	112	216	298	305	417	464	539		
						(615)	674	695	720	772	793	807		
						829	844	909	928	962				
352.6(2)	27(1)	<i>S</i>				154	385							
367.75(3)	80(2)	<i>S</i>	14.1(20)	<i>M1,E2</i>		188	239							
374.51(3)	90(2)	<i>S</i>	13.9(20)	<i>M1,E2</i>		115								
380.00(3)	28(1)	<i>S'</i>	13.8(40)	<i>M1,E2</i>		188	239	564						
384.85(6)	20(1)	<i>S</i>	12.1(60)	<i>M1,E2</i>		115	237	353						
388.9(1)	21(1)													
413.15(6)	30(3)	<i>S</i>	10.4(40)	<i>M1,E2</i>		104	188	239						
416.92(8)	13(1)	<i>S</i>	10.9(60)	<i>M1,E2</i>		273.6	324							
456.05(3)	184(3)	<i>S</i>	9.54(80)	<i>M1,E2</i>		115	318	474	539					
462.88(5)	117(3)	<i>S</i>	8.3(16)	<i>M1,E2</i>	*	112	115	488	634					
463.9(1)	3(2)	<i>S,N</i>				324								
473.90(6)	16(1)	<i>S'</i>				456								
488.33(4)	29(1)	<i>S'</i>				115	274	305	324	463				
506.7(2)	48(5)	<i>S</i>												
518.6(2)	15(5)	<i>S,N</i>				239								
527.7(1)	22(1)	<i>S,N</i>	5.5(20)	<i>M1,E2</i>	*	273.7								
538.6(2)	14(2)	<i>S',N</i>				456								
538.7(2)	7(1)	<i>S</i>				274	324							
540.7(4)	7(1)	<i>S</i>												
563.92(4)	132(4)	<i>S</i>	4.93(60)	<i>M1,E2</i>	*	188	239	380						
567.90(4)	33(2)	<i>S</i>			*									
571.42(3)	58(3)	<i>S</i>	4.9(10)	<i>M1,E2</i>		318	539							



TABLE I. (Continued).

$E_\gamma$ (keV)	$I_\gamma$ (relative)	ICC measurement		Former results	Coincident $\gamma$ rays (keV)	
		$10^3\alpha_k$	$\gamma$ multipol.			
1120.9(1)	46(3)	$N$				
1131.3(1)	50(4)	$S'$				
1136.5(1)	29(2)	$N$				
1141.5(1)	28(3)	$S', N$		239		
1153.9(1)	15(1)	$S'$				
1158.0(2)	15(3)	$S', N$		239		
1164.5(1)	32(2)	$S', N$		239		
1173.3(2)	14(5)	$S', N$		273.6	324	
1180.9(1)	66(3)	$N$				
1234.6(1)	30(3)	$N$				
1239.6(1)	35(3)	$N$				
1267.5(1)	27(2)	$N$				
1286.9(1)	26(2)	$N$				
1292.4(2)	28(2)	$N$				
1305.2(2)	32(2)	$N$				

TABLE II. Energies, relative intensities, internal conversion coefficients, multipolarities, and coincidence relations of  $\gamma$  rays of the  $^{115}\text{In}(\alpha, n\gamma)^{118}\text{Sb}$  reaction at  $E_\alpha = 14.5$  MeV. [ $S$ ,  $S'$ , and  $S''$  denote placement into the level schemes of Figs. 7, 8, and 9, respectively.  $N$  means a new  $\gamma$  ray. The asterisk means that multipolarity has been determined also from the  $(p, n\gamma)$  reaction in this work (see Table I)].

$E_\gamma$ (keV)	$I_\gamma$ (relative)	ICC measurement		Former results	Coincident $\gamma$ rays (keV)						
		$10^3\alpha_k$	$\gamma$ multipol.								
31.2(1)	$S$				239						
37.1(1)	$S'', N$				203	222	397	937			
50.8(1)	$S$			$E2$ [7]							
103.64(3)	90(5) $S$			$E1$ [10]	115	128	138	171.8	208	251	285
					304	413	423	901	908		
108.7(1)	6(1) $S'', N$				253	318					
110.5(1)	4(1) $S$				209	222	273.8	304			
112.3(1)	weak $S$				463						
115.37(3)	462(20) $S$	305(28)	$M1$	$M1$ [10]	104	112	128	138	154	158	172
				*	203.1	215	237	245.9	287	304	305
					357	375	385	413	423	456	463
					483	504	575	594.7	595.5	621	641
					692	716	755	833	878	901	
128.37(3)	443(20) $S$	240(28)	$M1$	*	104	115	138	171.8	188	208	238.6
					251	285	297	304	410	423	454
					594.7	682	761	766	812	813	901
					908	933	946				
138.15(3)	27(2) $S, N$				104	115	128	188	238.6	285	413
					694						
141.69(3)	38(2) $S, N$				273.8	294	568				
153.82(3)	62(3) $S$				115	203.1	237	295	306	315.6	353
					536	585.1	595.5				
158.19(8)	5(1) $S$				115						
171.7(1)	< 62 $S', N$				273.7	324	829				
171.8(1)	178(30) $S$	98(30)	$M1$		104	115	128	188	238.6	251	297
					304	366	594.7	642	682	761	812
177.03(7)	3(1) $S'', N$				253						
187.9(1)	39(6) $S$	26(4)	$E1$	*	128	138	171.8	368	413	423	
188.7(2)	17(1) $S'', N$				203	749					
202.7(1)	37(2) $S''$			$M1 + E2$ [13]	189	222	261	297	318	326	362
					397	415	619	676	715	744	749
					937						
203.1(1)	35(5) $S, N$				115	154	237	353	506		

TABLE II. (Continued).

$E_\gamma$ (keV)	$I_\gamma$ (relative)	ICC measurement $10^3\alpha_k$	$\gamma$ multipol.	Former results	Coincident $\gamma$ rays (keV)							
206.6(1)	weak											
208.2(2)	5(2)				128							
209.3(2)	160(9)	80(9)	$M1, E2$		110	222	273.8	304	415	577		
215.4(2)	5(2)				237							
216.28(3)	40(4)	71(12)	$M1, E2$	*	245.9	273.7	324	483	504	755		
222.33(10)	66(4)				110	209	274	303				
222.4(1)	73(3)				203	318	326	397	446	702	715	
224.35(3)	23(2)				229	273.8	304					
228.9(2)	6(2)				224	273.8	304	527.7				
232.65(5)	37(4)				203	273.8	585.2	596				
237.35(3)	232(30)				115	154	203.1	215	245.9	287	357	
					385	621	641	692				
238.57(3)	891(50)				128	138	171.8	208	239	251	285	
					300	304	368	379	413	423	436	
					528	564	594.7	682	716	747	803	
					812	813	855	901	908	933		
245.8(1)	10(5)				273.8							
245.9(1)	49(5)				115	216	237	287	353	375		
					483	621	973					
251.3(1)	31(3)				104	128	171.8	188	238.6			
253.41(4)	120(11)				109	177	318	572				
260.8(1)	28(3)				203	326	676					
273.7(1)	47(5)				171.1	216	305	720	829	844		
273.84(3)	1039(90)	32(5)	$M1, E2$		110	142	203	209	224	233	245.8	
					294	304	315.7	415	435.7	453	527.7	
					614	818	829	868	956			
284.84(4)	13(2)				104	115	128	138	238.6			
287.35(3)	21(2)				115	237	245.9	273.7	307	621	973	
294.1(1)	68(5)	25(5)	$M1$	*	142	273.8						
295.1(1)	8(1)				154	237	506					
297.1(1)	9(3)				203	318	322					
297.3(1)	weak				128	171.8	304					
300.0(1)	11(5)				238.6							
303.5(2)	320(50)				110	209	224	273.8	415	453	606	
303.6(1)	48(5)				104	115	128	171.8	238.6	297		
304.3(2)	30(6)											
304.8(2)	14(3)				112	273.7	324					
305.5(2)	20(10)				154	506	595					
310.3(1)	5(1)				318	397	577					
315.7(1)	31(3)				273.8	585	818					
318.23(3)	684(16)	25(3)	$M1, E2$		109	177	203	222	253	297	310	
					322	326	371	376	392	397	430	
					446	572	577	579	584	619	747	
					793	837.1	872	883	1014	1072		
321.94(7)	54(3)				297	318						
324.28(3)	121(5)	22(3)	$M1(+E2)$	*	171.7	216	305	674	720	829	844	
326.3(2)	24(1)				203	222	261	362	937	1177		
352.62(8)	39(3)				154	203.1	245.9	621	641			
357.1(2)	8(2)				115	237						
358.3(4)	5(1)				261	318						
362.2(1)	9(1)				203	326	1177					
367.73(3)	88(4)				188	238.6	558					
371.06(3)	73(2)				318	376	392	397	516	715	769	
374.51(4)	93(4)				115	245.9	287	483	504	573	755	
376.17(4)	16(1)				318	371	392	397				
379.43(5)	27(2)				238.6	564						
385.0(1)	5(2)				237							
392.4(1)	5(1)				318	371	376	397				
396.65(4)	197(8)	4.6(8)	$E1+M2$		203	222	310	318	326	371	376	
					392	577	747	837.4				

TABLE II. (Continued).

$E_\gamma$ (keV)	$I_\gamma$ (relative)	ICC measurement		Former results	Coincident $\gamma$ rays (keV)						
		$10^3\alpha_k$	$\gamma$ multipol.								
410.1(1)	4(1) $S,N$				128						
413.2(1)	128(5) $S$	10(2)	$M1,E2$		104	115	138	188	238.6	528.5	
415.5(1)	3(1) $S'',N$				203	1177					
422.96(3)	36(2) $S,N$	9(3)	$(M1,E2)$		104	115	128	188	238.6		
430.4(1)	6(1) $S'',N$				318						
435.7(1)	17(3) $S,N$				273.8						
446.49(6)	7(1) $S'',N$				189	222	261	318	397	937	
453.3(1)	70(4) $S',N$	9.2(19)	$M1,E2$		273.8	304	577				
454.2(1)	3(1) $S,N$				128	238.6					
456.1(2)	15(3) $S$			*	115						
462.85(5)	67(5) $S$	7.9(14)	$M1,E2$	*	112	115					
483.4(1)	15(2) $S',N$				115	216	245.9	287	324	375	
488.3(3)	<22 $S'$										
503.7(1)	9(4) $S',N$				375						
506.4(2)	230(99) $S$				203.1	295	306	315.6	536	585.1	595.5
516.3(1)	4(1) $S'',N$										
527.7(1)	87(8) $S,N$	5.6(14)	$M1,E2$	*	229	273.8					
528.4(1)	3(2) $S',N$				238.6	413					
536.4(1)	6(2) $S',N$				115	154	237	506			
551.29(7)	7(2) $S,N$				238.6						
558.46(5)	11(2) $S',N$				238.6	368					
563.90(5)	29(3) $S$	4.4(14)	$M1,E2$	*	188	238.6	379				
567.94(3)	130(5) $S$	4.8(8)	$M1,E2$		142						
571.7(1)	15(2) $S'',N$				253	318	571.9				
571.9(1)	21(2) $S'',N$				109	177	571.7				
572.9(1)	8(3) $S',N$				216	375					
575.1(2)	6(2) $S$			*	115						
577.2(2)	<29 $S'',N$				310	318	397	715			
577.3(2)	<29 $S$				209	453					
579.47(3)	63(2) $S'',N$				318						
583.7(3)	8(1) $S'',N$										
585.1(1)	7(2) $S',N$				115	154	237	506			
594.7(1)	18(3) $S',N$				104	115	128	171.8	238.6		
595.5(1)	16(5) $S',N$				115	154	237	306	353	506	
605.5(1)	7(2) $S',N$				273.8	304					
614.36(3)	27(2) $S$	5.0(13)	$M1(+E2)$	*	273.8						
619.0(1)	12(1) $S',N$				203	318					
620.7(1)	40(3) $S',N$				115	237	245.9	2877	353		
637.02(7)	7(2) $S'',N$				749						
640.87(6)	30(3) $S',N$	2.9(14)	$M1,E2$	*	115	237	353				
641.7(2)	6(3) $S',N$				104	115	128	171.8			
674.2(1)	15(3) $S$			*	273.7	324					
676.49(4)	19(1) $S'',N$				203	261					
680.23(3)	71(3) $S'',N$				793						
690.(1)	10(5) $S$			*							
701.8(2)	5(2) $S'',N$				222	261	318	397	937		
714.9(1)	58(5) $S'',N$				222	371	376	577			
715.5(1)	18(3) $S$				104	115	238.6				
719.86(5)	18(2) $S'$			*	273.7	324					
737.49(4)	19(2) $S$			*							
744.5(1)	9(1) $S'',N$				203						
747.0(1)	3(2) $S'',N$				392	397	715				
747.3(1)	17(5) $S'$			*	188	238.6					
748.5(1)	73(3) $S'',N$			*	189	203	637				
755.3(1)	15(2) $S',N$			*	115	216	375				
761.31(7)	13(2) $S',N$				128	171.8	238.6				
763.8(1)	5(1) $S'',N$										
766.3(1)	4(1) $S',N$				128	238.6					

TABLE II. (Continued).

$E_\gamma$ (keV)	$I_\gamma$ (relative)	ICC measurement		Former results	Coincident $\gamma$ rays (keV)					
		$10^3\alpha_k$	$\gamma$ multipol.							
768.9(1)	5(1)	$S'',N$			371					
788.2(2)	14(1)	$S$		*						
793.3(2)	8(2)	$S'$		*	273.7	324				
803.13(5)	23(3)	$S'$		*	188	238.6				
811.7(1)	4(1)	$S',N$			104	128	171.8	238.6		
813.1(1)	10(2)	$S',N$			104	115	128	188	238.6	
817.9(1)	38(4)	$S',N$			273.8	316				
829.14(7)	38(7)	$S'$			171.7	273.7	324			
832.6(1)	19(3)	$S$			115					
837.1(1)	21(2)	$S'',N$		*	318					
837.4(1)	6(3)	$S'',N$			318	397				
844.1(1)	10(2)	$S',N$			273.8	324				
854.62(5)	26(3)	$S',N$			104	115	188	238.6		
867.5(2)	20(3)	$S',N$		*	273.8					
872.3(1)	4(2)	$S'',N$			253	318				
878.1(1)	7(1)	$S'$		*	115					
882.82(6)	6(2)	$S'',N$			318					
901.36(5)	26(3)	$S',N$			104	115	128	188	238.6	
908.4(2)	24(3)	$S',N$			104	115	128	188	238.6	
933.17(9)	7(1)	$S',N$			128	238.6				
937.17(4)	95(4)	$S'',N$	1.9(3)	$M1$	203	326				
943.6(1)	31(4)	$S'$		*	239					
955.6(1)	12(2)	$S',N$		*	273.8					
962.2(1)	10(2)	$S'$								
973.15(7)	23(2)	$S',N$			245.9	287				
1014.0(1)	8(2)	$S'',N$			318					
1039.6(12)	17(2)	$S',N$			238.6					
1044.5(1)	15(2)	$S'$								
1067.9(2)	10(2)	$S'',N$			318					
1072.0(1)	5(1)	$S'',N$			318					
1153.9(1)	30(2)	$S'$			171.7					
1177.1(1)	20(2)	$S'',N$			326	362	415			
1201.6(3)	5(1)	$S'',N$								

tions to the experimental ones are shown in Fig. 4. Only those spin and parity values have been considered for initial states which were not in contradiction with the results of internal conversion coefficient measurements. Spins were rejected on the basis of a 0.1% confidence limit for the reduced  $\chi^2$  fits. The error limits of the multipole mixing ratio ( $\delta$ ) correspond to  $\chi^2_{\min} + 1$  values. The results of the  $\gamma$ -ray angular distribution measurements are summarized in Table III.

#### IV. LEVEL SCHEME OF $^{118}\text{Sb}$

The level schemes were based mainly on  $\gamma\gamma$ -coincidence measurements, as well as on the energy and intensity balance of transition. The proposed level scheme from the  $(p,n\gamma)$  reaction is shown in Figs. 5 (low-energy part) and 6 (high-energy part). The level scheme obtained from the  $(\alpha,n\gamma)$  reaction can be seen in Figs. 7 (low-energy part), 8 (levels up to 1.5 MeV), and 9 (levels based on the 212-keV  $8^-$  isomeric state).

The spins and parities have been determined on the basis of the decay properties of the levels from the measured internal conversion coefficients (in both reactions),

as well as from Hauser-Feshbach analysis and  $\gamma$ -ray angular distribution results [in the  $(p,n\gamma)$  reaction]. Arguments used for spin and parity assignments are summarized in Table IV.

Comparisons between the low-spin-level spectra, obtained from the  $(p,n\gamma)$  and  $(\alpha,n\gamma)$  reactions, are given in Figs. 6 and 8. There are naturally many similarities between the level schemes, but the 628.0-keV ( $5^+$ ), 760.4-keV (4,3), 808.2-keV (3-5), 821.1-keV ( $3^-5^-$ ), 837.4-keV ( $6^+$ ), 873.4-keV, and 947.9-keV, mainly medium-spin levels were observed only in the  $(\alpha,n\gamma)$  reaction, while the 863.4-keV ( $2^+$ ), and 940.1-keV (0,2,3) low-spin states were not seen here. Above 1 MeV excitation energy, there are many differences.

The proposed level scheme from the  $(p,n\gamma)$  reaction is in general agreement with that of Chaffee [3]. The most striking difference (apart from the more definite spin and parity determinations) is that the 324.6-, 557.4-, and 618.7-keV levels and related  $\gamma$  transitions are shifted up by 51 keV. Thus the 273.7-keV transition is feeding the 50.8-keV  $3^+$  level instead of the  $1^+$  ground state (Fig. 5). The necessity of such a displacement follows from the higher ( $> 3$ ) spin of the 324.6-keV level, which is suggest-

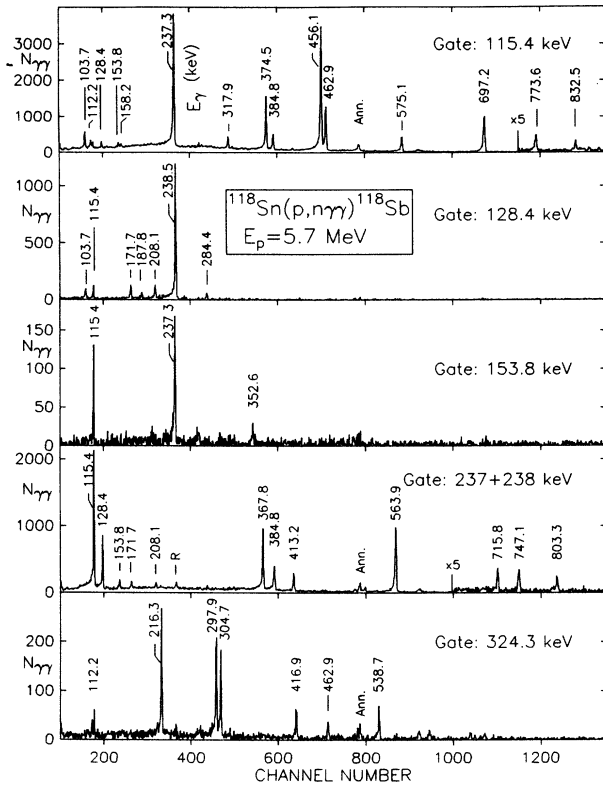


FIG. 3. Typical  $\gamma\gamma$ -coincidence spectra measured with Ge(HP) and Ge(HP,LEPS) detectors. The background was subtracted. *R* denotes random coincidences.

ed by the low relative ( $p,n$ ) and higher ( $\alpha,n$ ) cross sections of the state. An  $M1, E2$  transition from this state to the  $1^+$  ground state is impossible. In our level scheme, the 557.4-keV level decays by 506.7-, 232.8- and 153.78-keV transitions; the position of the latter is based on coincidence relations in the ( $p,n\gamma$ ) reaction. The  $\gamma$ -branching ratios from the 557.4-keV level in different reactions and at different bombarding particle energies agree fairly well, too. Confirmation of the position of the 557.2-keV level could be deduced also from  $\gamma\gamma$ -coincidence measurement in a ( $\alpha,n\gamma$ ) reaction, because all the transitions feeding the 557.2-keV level in Fig. 7 are in coincidence both with the 506.4- and 153.82-keV transitions, while the position of the latter is proved by other unambiguous evidence. The possibility of this displacement is also indicated in Chaffee's work [3] and does not contradict his excitation function measurements.

Still remarkable differences between Chaffee's and our level scheme are as follows: (a) We have found that Chaffee's 304.5-keV line [3], deexciting the 629.1-keV state, is actually a doublet. (b) The 614.39-keV transition from the 939.0-keV level feeds the 324.6-keV (shifted) state instead of the 324.3-keV level. The (a) and (b) conclusions have been drawn on the basis of the transition intensity ratios, observed in the coincidence spectra at 274- and 324-keV gates. (c) We have introduced the 606.3- and 852.3-keV levels and have not seen the 507.7-keV state.

The  $\gamma$ -ray branching ratios indicated in Figs. 5–8 are averages of results obtained at different bombarding pro-

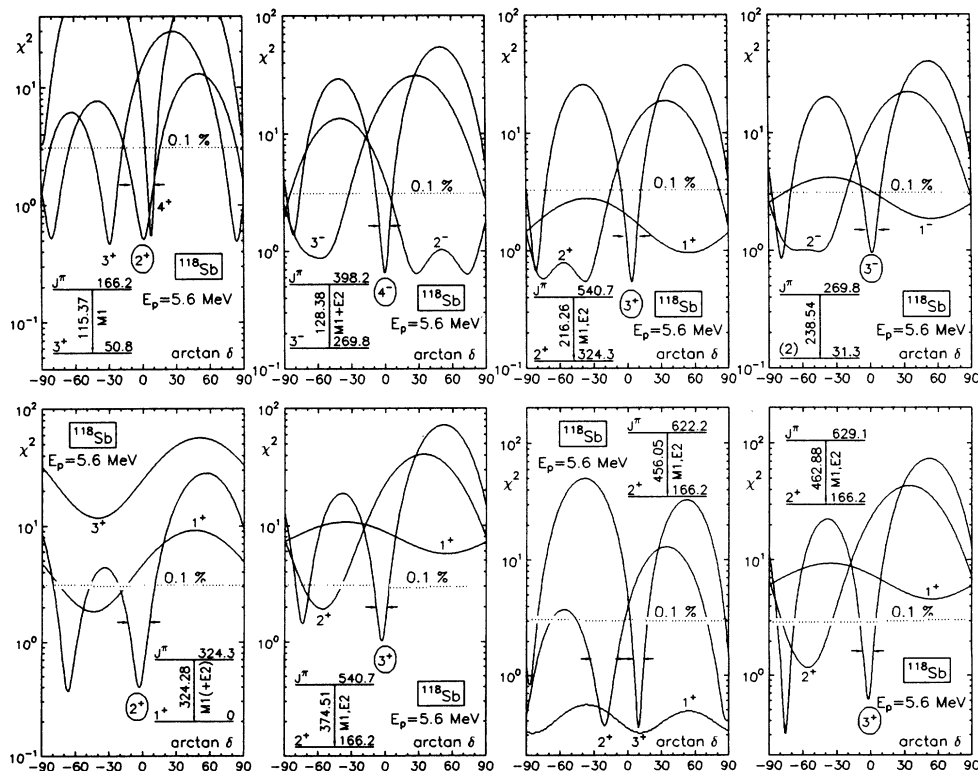


FIG. 4. Reduced  $\chi^2$ -test plots of  $^{118}\text{Sb}$  transitions (indicated in the insets) as a function of  $\arctan\delta$ , where  $\delta^2$  is the  $E2/M1$  intensity ratio for the transition. Labeled numbers are assumed spins and parities for the initial state in question. Encircled numbers are adopted spins and parities based on all available data. The dashed lines show the 0.1% confidence limits for reduced  $\chi^2$ .





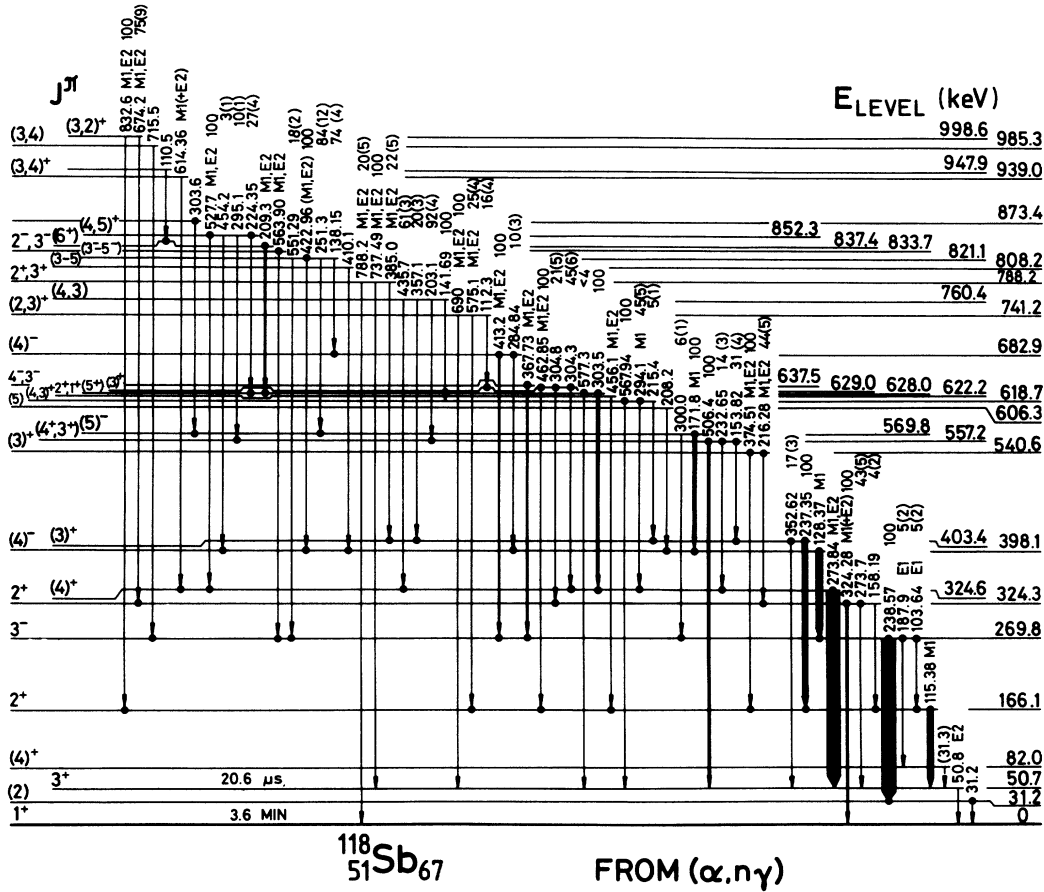


FIG. 7. Low-energy part of the proposed level scheme of  $^{118}\text{Sb}$  from the  $^{115}\text{In}(\alpha, n\gamma)^{118}\text{Sb}$  reaction. Solid circles at the ends of arrows indicate  $\gamma\gamma$ -coincidence relations. After the energies of the transitions, multipolarities and  $\gamma$ -ray branching ratios are given.

TABLE IV. Spin and parity ( $J^\pi$ ) assignments to  $^{118}\text{Sb}$  levels. [If the level was observed in both the  $(p, n\gamma)$  and  $(\alpha, n\gamma)$  reactions, an asterisk was placed after the level energy.]

Level energy (keV)	$J^\pi$	Basis of the $J^\pi$ assignment, comments
0*	1 <sup>+</sup>	$J=1$ from atomic-beam magnetic-resonance measurement [6]. $\log ft=4.5$ EC+ $\beta^+$ transition to $^{118}\text{Sn}$ 0 <sup>+</sup> ground state [5].
31.3*(1)	(2)	Predominantly dipole character of the 31-keV $\gamma$ ray, feeding the 1 <sup>+</sup> ground state [10]. Expected 2 <sup>-</sup> member of the $\pi g7/2\nu h11/2$ multiplet (parabolic rule and IBFFM calculations).
50.8*(1)	3 <sup>+</sup>	Pure E2 transition to the 1 <sup>+</sup> ground state, magnetic-moment measurement established [ $\pi d5/2\nu s1/2$ ] <sub>+</sub> configuration [7].
82.1*(2)	(4) <sup>+</sup>	The level is fed by a E1 188-keV transition from the 3 <sup>-</sup> state, no transition to the 1 <sup>+</sup> ground state, angular distribution of the 188-keV $\gamma$ ray, systematics of low-lying levels in odd-odd Sb nuclei.

TABLE IV. (Continued).

Level energy (keV)	$J^\pi$	Basis of the $J^\pi$ assignment, comments
166.2*(1)	$2^+$	115-keV $M1$ transition to $3^+$ state, 115-keV $\gamma$ -ray angular distribution; Dima <i>et al.</i> [10] give $J^\pi=2^+$ . Parabolic rule and IBFFM calculations predict a $[\pi d5/2\nu s1/2]_{2^+}$ configuration for the state.
269.8*(1)	$3^-$	$E1$ transitions to $2^+$ [and $(4)^+$ ] states, angular distributions of the 104- and 239-keV $\gamma$ rays, Hauser-Feshbach analysis; Dima <i>et al.</i> [10] give $3^-$ . Parabolic rule and IBFFM calculations predict a $[\pi d5/2\nu h11/2]_{3^-}$ configuration for the state. Systematics of the odd-odd Sb nuclei.
324.3*(1)	$2^+$	$M1(+E2)$ transition to the $1^+$ ground state, transitions to $3^+$ and $2^+$ states, angular distribution of the 324-keV $\gamma$ ray.
324.6*(1)	$(4)^+$	$M1, E2$ transition to the $3^+$ state, Hauser-Feshbach analysis; the level was excited more intensively from the $(\alpha, n\gamma)$ reaction.
398.2*(1)	$(4)^-$	$M1(+E2)$ transition to the $3^-$ state, Hauser-Feshbach analysis, angular distribution of the 128-keV $\gamma$ ray. Parabolic rule and IBFFM calculations suggest a $[\pi d5/2\nu h11/2]_{4^-}$ configuration.
403.5*(1)	$(3)^+$	Transitions to $3^+$ and $2^+$ states. The level is fed by $M1, E2$ transition from the 788-keV positive-parity level. Hauser-Feshbach analysis.
540.7*(1)	$(3)^+$	$M1, E2$ transition to $2^+$ states, transition to the $1^+$ ground state, Hauser-Feshbach analysis, angular distribution of the 216-keV $\gamma$ ray.
557.4*(1)	$(4^+, 3^+)$	Transitions to $3^+$ , $(4)^+$ , and $(3)^+$ states, Hauser-Feshbach analysis.
569.9*(2)	$(5)^-$	$M1$ transition to the $(4)^-$ state, transition to the $3^-$ state [from the $(\alpha, n\gamma)$ reaction], Hauser-Feshbach analysis, expected $5^-$ member of the $\pi d5/2\nu h11/2$ multiplet.
606.3*(2)	$(5)$	Transition to the $(4)^-$ state, Hauser-Feshbach analysis.
618.7*(1)	$(4, 3)^+$	$M1$ transition to the $(4)^+$ state, transitions to $3^+$ and $(3)^+$ states, Hauser-Feshbach analysis.
622.2*(1)	$2^+, 1^+$	$M1, E2$ transitions to $2^+$ and $3^+$ states, $M1(+E2)$ transition to the $1^+$ ground state, transition to the $2^+$ state, Hauser-Feshbach analysis, angular distribution of the 298-, 456-, 571-, and 622-keV $\gamma$ rays.

TABLE IV. (*Continued*).

Level energy (keV)	$J^\pi$	Basis of the $J^\pi$ assignment, comments
628.0(2)	(5 <sup>+</sup> )	Strong transition to the (4) <sup>+</sup> and weak transition to the 3 <sup>+</sup> states. It is not seen in the ( $p,n\gamma$ ) reaction, which indicates higher spin. Parabolic rule and IBFFM calculations suggest a $[\pi 5/2\nu g 7/2]_{5+}$ configuration.
629.1*(1)	(3) <sup>+</sup>	$M1, E2$ transitions to 2 <sup>+</sup> and 3 <sup>+</sup> states, transitions to 2 <sup>+</sup> and (4) <sup>+</sup> states, Hauser-Feshbach analysis, angular distribution of the 463-keV $\gamma$ ray.
637.6*(1)	4 <sup>-</sup> , 3 <sup>-</sup>	$M1, E2$ transition to the 3 <sup>-</sup> state, Hauser-Feshbach analysis.
683.0*(1)	(4) <sup>-</sup>	$M1, E2$ transition to the 3 <sup>-</sup> state, transition to the (4) <sup>-</sup> state, Hauser-Feshbach analysis.
741.3*(1)	(2,3) <sup>+</sup>	$M1, E2$ transitions to 3 <sup>+</sup> and 2 <sup>+</sup> states, transition to the (3) <sup>+</sup> state, Hauser-Feshbach analysis, no transition to the 1 <sup>+</sup> ground state, angular distribution of the 575- and 690-keV $\gamma$ rays.
760.4(1)	(4,3)	Transitions to the (4) <sup>+</sup> , (3) <sup>+</sup> , (4 <sup>+</sup> , 3 <sup>+</sup> ), and (4,3) <sup>+</sup> states.
788.3*(1)	2 <sup>+</sup> , 3 <sup>+</sup>	$M1, E2$ transitions to 1 <sup>+</sup> , 3 <sup>+</sup> , and (3) <sup>+</sup> states, transitions to 2 <sup>+</sup> and 3 <sup>-</sup> states, Hauser-Feshbach analysis.
808.2(2)	(3-5)	Transition to the (4) <sup>-</sup> state.
821.1(1)	(3 <sup>-</sup> -5 <sup>-</sup> )	Transitions to 3 <sup>-</sup> , (4) <sup>-</sup> , (5) <sup>-</sup> , and (4) <sup>-</sup> states.
833.8*(1)	2 <sup>-</sup> , 3 <sup>-</sup>	$M1, E2$ transition to the 3 <sup>-</sup> state, Hauser-Feshbach analysis, angular distribution of the 564-keV $\gamma$ ray.
837.4(2)	(6 <sup>+</sup> )	$M1, E2$ transition to the (5 <sup>+</sup> ) level. Missing of the state in the ( $p,n\gamma$ ) reaction indicates higher spin. Parabolic rule and IBFFM calculations suggest a $[\pi d 5/2\nu g 7/2]_{6+}$ configuration for this state.
852.3*(2)	(4,5) <sup>+</sup>	$M1, E2$ transition to the (4) <sup>+</sup> state, transitions to (4) <sup>-</sup> , (4 <sup>+</sup> , 3 <sup>+</sup> ), and (5 <sup>+</sup> ) states [from the ( $\alpha,n\gamma$ ) reaction], Hauser-Feshbach analysis.
863.4(1)	(2) <sup>+</sup>	$M1, E2$ transitions to 1 <sup>+</sup> and 2 <sup>+</sup> states, transition to the 2 <sup>+</sup> state, Hauser-Feshbach analysis.
873.4(2)		
939.0*(2)	(3,4) <sup>+</sup>	$M1(+E2)$ transition to the (4) <sup>+</sup> state, Hauser-Feshbach analysis.
940.1(1)	(0,2,3)	Transitions to 1 <sup>+</sup> , 2 <sup>+</sup> , and 2 <sup>+</sup> , 1 <sup>+</sup> states, Hauser-Feshbach analysis.
947.9(2)		
985.6*(2)	(3,4)	Transition to the 3 <sup>-</sup> state, Hauser-Feshbach analysis.
998.7*(1)	(3,2) <sup>+</sup>	$M1, E2$ transitions to 2 <sup>+</sup> states, Hauser-Feshbach analysis.

TABLE IV. (Continued).

Level energy (keV)	$J^\pi$	Basis of the $J^\pi$ assignment, comments
> 1000		Spin and parity assignments above 1000 keV excitation energy are based on decay properties of levels [transitions, multiplicities; see $(p, n\gamma)$ and $(\alpha, n\gamma)$ level schemes]. The errors of level energies, not indicated, are less than 0.2 keV.

ton energies and in the  $(\alpha, n\gamma)$  reaction. Apart from the differences mentioned above, the derived branching ratios are in satisfactory agreement with the results of Chaffee [3].

The high-spin levels, decaying onto the 212-keV  $8^-$  5.0-h isomeric state [13], are shown in Fig. 9. The 1186.3-keV ( $8^-$ ), 1389.1-keV ( $9^-$ ), 1715.3-keV ( $10^-$ ), and 2077.5-keV ( $11^-$ ) states correspond to the members of the high-spin intruder band, identified by Vajda *et al.*

[4]. The levels decay with the same  $\gamma$  cascade as in [4]. The only exception is the 1149.2-keV  $(7, 8)^-$  state, which decays by a 222.4-keV (instead of 197-keV) transition to the 926.9-keV  $(7)^+$  level. This means a  $\sim 26$ -keV shift in level energies, which is confirmed by the existence of the 937.17- and 1177.1-keV crossover transitions from the 1149.2-keV  $(7, 8)^-$  and 1389.1-keV ( $9^-$ ) levels, respectively. Transitions, connecting the low- and high-spin parts of the level scheme, were not found.

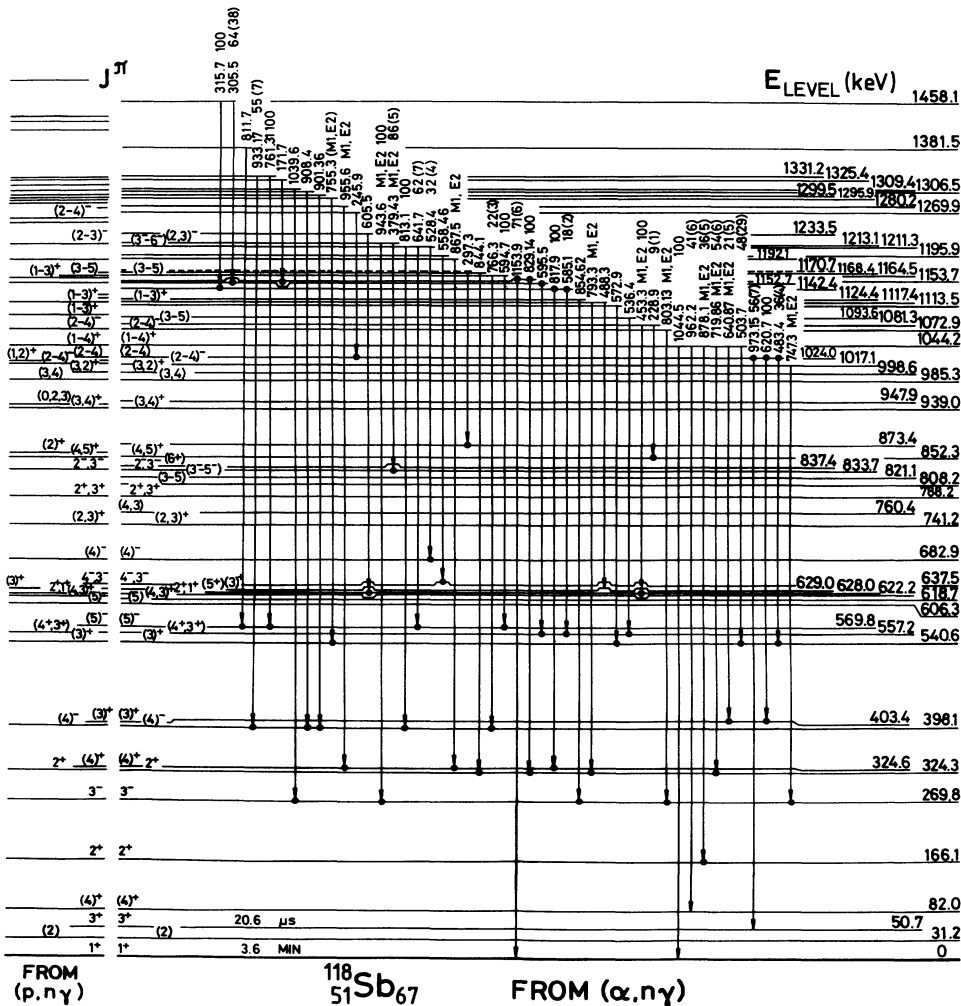


FIG. 8. High-energy part of the proposed level scheme of  $^{118}\text{Sb}$ . Left side: levels from our  $(p, n\gamma)$  measurements.

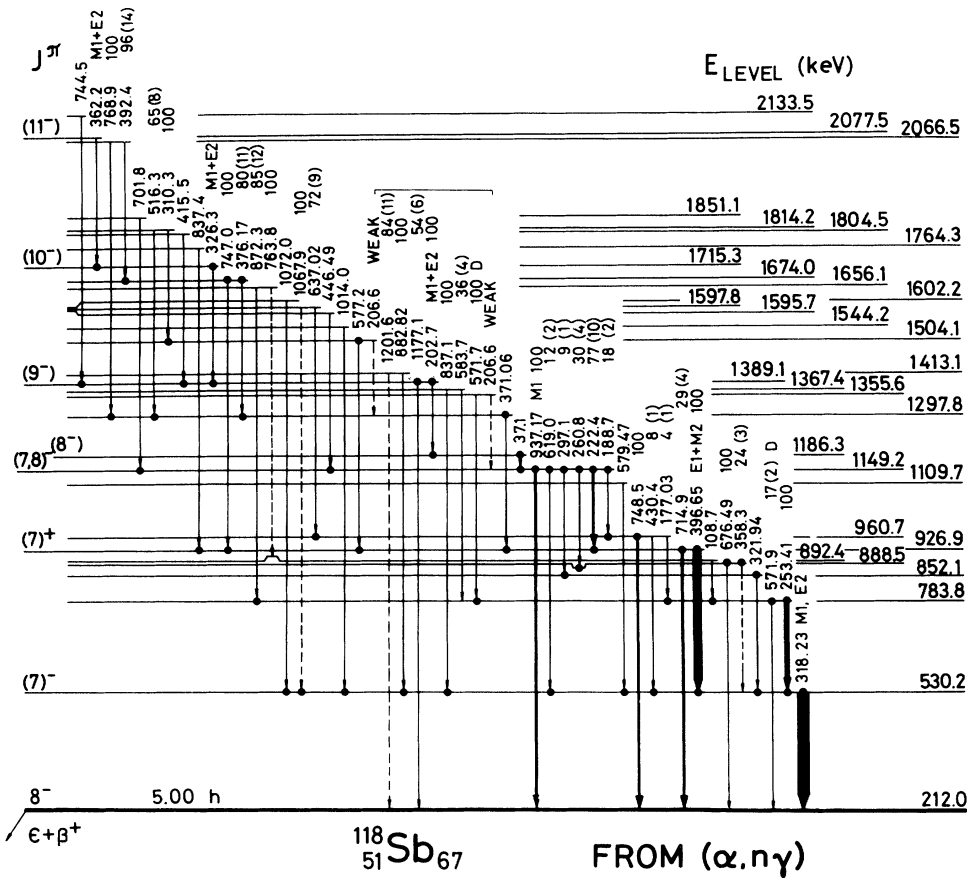


FIG. 9. Proposed high-spin level scheme of  $^{118}\text{Sb}$ , based on the  $8^-, 5.0\text{ h}$  isomeric state [from the  $^{115}\text{In}(\alpha, n\gamma)^{118}\text{Sb}$  reaction]. Solid circles at the ends of arrows indicate  $\gamma\gamma$ -coincidence relations. After the energies of the transitions, multipolarities and  $\gamma$ -ray branching ratios are given. *D* denotes double placement.

## V. HAUSER-FESHBACH ANALYSIS

As a result of detailed  $\gamma$ - and  $e^-$ -spectroscopic measurements, the low-spin, low-energy ( $E_{\text{lev}} < 1\text{ MeV}$ ) level scheme of  $^{118}\text{Sb}$  can be considered nearly complete. Thus the  $(p, n)$  cross sections for the neutron groups feeding the  $^{118}\text{Sb}$  levels could be deduced from transition intensities between excited states. The obtained  $\sigma_{\text{lev}}(p, n)$  relative cross sections are shown in Fig. 10 (dots with error bars). In order to support the level spin determination,  $\sigma_{\text{lev}}(p, n)$  values were calculated at 5.7 and 6.0 MeV ingoing proton energies using the CINDY [17] program, which is based on the compound nuclear reaction model. The transmission coefficients were calculated using the optical-model parameter set of Wilmore and Hodgson [21] for neutrons and of Józsa *et al.* [22] for protons. Józsa *et al.* determined the optical-model potential parameters for  $p + ^{118}\text{Sn}$  scattering close to the proton energies that were used in our experiments. The parameters of the optical potentials are given in Table V. In addition to the neutron channels, the strongest  $(p, p')$  channels

were included. The Moldauer width fluctuation correction [17] was also taken into account. The experimental and theoretical cross sections were normalized at the 166-keV  $2^+$  and 324-keV  $2^+$  states. The theoretical results (curves) are compared with the experimental ones in Fig. 10. As seen in the figure, the possible spin region for a level can be limited to one or two spins (below 1 MeV excitation energy and  $J \leq 5$ ). The possible spins were usually consistent with the results obtained by other methods. Nevertheless, the present Hauser-Feshbach analysis results were used only for confirming and reducing the spin regions, because of the relatively large experimental errors of normalization points. An exception is the 325-keV (shifted) level, where the Hauser-Feshbach analysis suggests a  $J=4, 5$  spin value, which is a fundamental reason for the displacement of the level. A similar Hauser-Feshbach analysis has been performed in our former work [33] for the analogous  $^{116}\text{Sb}$  nucleus. The level spins, obtained from the analysis, were consistent with other results. The parities were determined usually from the multipolarity of transitions.

TABLE V. Optical-model potential parameters used in this work [21,22]. (The  $V$ ,  $W$ , and  $V_{\text{s.o.}}$  potential depths are given in MeV and the  $r$  range and  $a$  diffuseness parameters in fm.)  $E$  is the energy of ingoing proton and outgoing neutron in MeV.

	$V$	$W$	$V_{\text{s.o.}}$	$r_{\text{Re}}$	$r_{\text{Im}}$	$a_{\text{Re}}$	$a_{\text{Im}}$
$p + ^{118}\text{Sn}$	$64.13 - 1.02E$	14.22	7.5	1.25	1.25	0.65	0.47
$n + ^{118}\text{Sb}$	$47.01 - 0.27E - 0.0018E^2$	$9.52 - 0.53E$	7.5	1.27	1.24	0.66	0.48

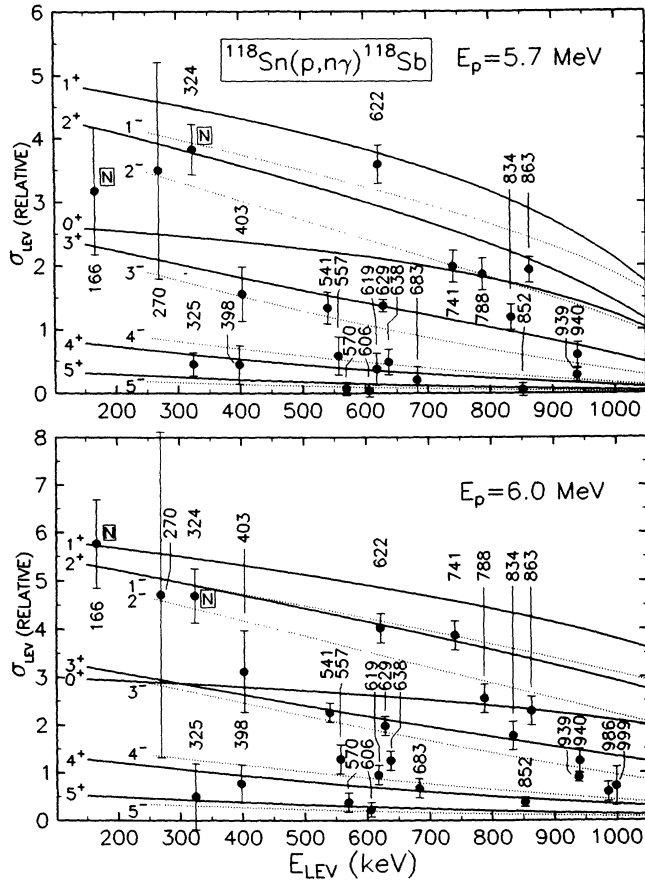


FIG. 10. Experimental relative cross sections ( $\sigma_{lev}$ ) of the  $^{118}\text{Sn}(p, n\gamma)^{118}\text{Sb}$  reaction (dots with error bars) as a function of the  $^{118}\text{Sb}$  level energy ( $E_{lev}$ ). The solid and dotted lines show Hauser-Feshbach theoretical results. *N* means normalization point.

VI. PROTON-NEUTRON MULTIPLET STATES, PARABOLIC RULE CALCULATIONS

In the  $^{118}\text{Sb}_{67}$  nucleus, one can expect excitations of the odd proton and odd neutron, and the coupling of different single-particle states.

The low-lying states of the neighboring  $^{117}\text{Sb}_{66}$  and  $^{117}\text{Sn}_{67}$  nuclei are shown in Fig. 11(a). Since in antimony there is only one proton beyond the  $Z = 50$  closed shell, the lowest-lying states have mainly single-proton configurations. According to the ( $^3\text{He}, d$ ) [23,24] and ( $\alpha, t$ ) [25] proton-transfer reaction studies, the ground  $\frac{5}{2}^+$ , 527-keV  $\frac{7}{2}^+$ , and 1322-keV  $\frac{11}{2}^-$  states carry the largest fractions of the  $\pi d5/2$ ,  $\pi g7/2$ , and  $\pi h11/2$  proton single-particle strengths, respectively. The 720-keV  $\frac{1}{2}^+$  state has large  $\pi s1/2$  components, but the  $\pi d5/2 \times 2^+$  one-phonon component is also strong. Similarly, the 924-keV  $\frac{3}{2}^+$  state has a substantial  $\pi d3/2$  component, but the  $\pi(g7/2 + d5/2) \times 2^+$  components are dominating (see also calculations of Kisslinger and Sorensen cited in [24]). The 1160-keV  $\frac{9}{2}^+$  state has  $g_{9/2}^{-1}$  proton-hole character (intruder state with strong deformation [26,27]).

The ( $d, p$ ) neutron-transfer experiments of Schneid, Prakash, and Cohen [28] and Carson and McIntyre [29] show that the  $\nu s1/2$ ,  $\nu d3/2$ ,  $\nu h11/2$ , and  $\nu g7/2$  spectroscopic strengths are concentrated in the ground  $\frac{1}{2}^+$ , 159-keV  $\frac{3}{2}^+$ , 315-keV  $\frac{11}{2}^-$ , and 712-keV  $\frac{7}{2}^+$  states of  $^{117}\text{Sn}$ , respectively. On the basis of Coulomb excitation and nucleon-transfer studies, Stelson *et al.* [30] concluded that the 1005-keV  $\frac{3}{2}^+$  state has  $\nu s1/2 \times 2^+$ , the 1020-keV  $\frac{5}{2}^+$  state  $\nu d5/2 + s1/2 \times 2^+$ , and the 1180-keV  $\frac{5}{2}^+$  state  $\nu d3/2 \times 2^+ + d5/2^+$  dominating configurations.

By the use of the "parabolic rule" [31], we have calculated the energy splitting of different proton-neutron multiplets as a function of  $J(J+1)$ , where  $J$  is the spin of the

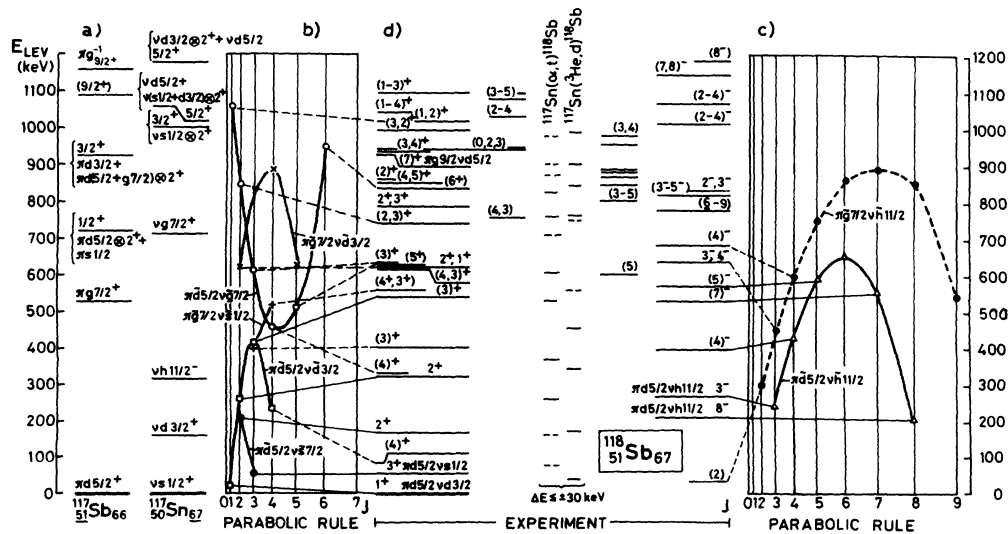


FIG. 11. Proton-neutron multiplet states in  $^{118}\text{Sb}$ . (a) Experimental level energies and configurations of the lowest-lying states of  $^{117}\text{Sb}$  and  $^{117}\text{Sn}$  nuclei. (b),(c) Results of the parabolic rule calculation for positive- and negative-parity states, respectively. The abscissa is scaled according to  $J(J+1)$ , where  $J$  is the spin of the state. (d) Experimental results on  $^{118}\text{Sb}$  levels.

state. The calculations were performed in a similar way as in the case of  $^{112}\text{In}$  using the same formulas [32]. The parameters of the calculations were as follows: quadrupole coupling strength,  $\alpha_2^0=4.4$  MeV; spin vibrational coupling strength,  $\alpha_1^0 \approx 15/A=0.13$  MeV; and occupation probabilities of quasineutron states,  $V^2(vd5/2)=0.88$ ,  $V^2(vg7/2)=0.85$ ,  $V^2(vs1/2)=0.51$ ,  $V^2(vd3/2)=0.30$ , and  $V^2(vh11/2)=0.23$ . The  $V^2$  values were taken from a systematics of experimental data (citations in [32]).

The results of calculations are presented in Figs. 11(b) and 11(c). We used at each multiplet one overall normalization term, which pushed up (or down) all members of the given multiplet with the same energy.

The experimental data are presented in Fig. 11(d). The level energies, spins, and parities are shown on the basis of our  $(p, n\gamma)$  and  $(\alpha, n\gamma)$  results; the main configurations are based on nuclear magnetic-moment measurements [12]. The  $(\alpha, t)$  and  $(^3\text{He}, d)$  proton-transfer reaction data show the preliminary results of Chaffee [3].

Between the neighboring  $J$  and  $J \pm 1$  members of the same  $p$ - $n$  multiplet, one can expect  $M1$  transitions. In order to facilitate configuration assignments, we have presented the decay properties of some low-lying states of  $^{118}\text{Sb}$  in Fig. 12.

**The  $\pi 5/2\nu\bar{s}1/2$  doublet.** The magnetic-moment measurements of Ploşinaru *et al.* [7] show that the main configuration of the 51-keV  $3^+$  level is  $\pi d5/2\nu\bar{s}1/2$ . Both the 51-keV  $3^+$  and 166-keV  $2^+$  levels were excited in the  $^{117}\text{Sn}(^3\text{He}, d)^{118}\text{Sb}$  proton-transfer reaction [3], suggesting a  $\nu s1/2$  dominating configuration for these states. The 166-keV  $2^+$  level decays only to the 51-keV  $3^+$  state by an intramultiplet  $M1$  transition. The parabolic rule calculation predicts that  $E_{\text{lev}}(2_1^+) > E_{\text{lev}}(3_1^+)$ , in accor-

dance with the experimental data.

**The  $\pi d5/2\nu\bar{d}3/2$  multiplet.** On the basis of nuclear magnetic-moment measurements, Jackson, Rogers, and Garrett [6] suggested a  $\pi d5/2\nu\bar{d}3/2$  configuration for the  $1^+$  ground state of  $^{118}\text{Sb}$ . According to the parabolic rule calculation, the lowest-energy member of the multiplet is the  $1_1^+$  state, and good candidates for the  $2^+$ ,  $3^+$ , and  $4^+$  multiplet members are the 324.3-keV  $2^+$ , 541-keV  $(3^+)$ , and 82-keV  $(4^+)$  levels. Similar parabolic energy splitting of the  $\pi d5/2\nu\bar{d}3/2$  multiplet has been observed also in  $^{116}\text{Sb}$  [33] and  $^{120}\text{Sb}$  [34]. The  $1^+$  ground state is fed by a strong  $M1(+E2)$  transition from the 324.3-keV  $2^+$  level and by a crossover transition from the 541-keV  $(3^+)$  state, while the 541-keV  $(3^+)$  state decays by a strong  $M1, E2$  transition to the 324.3-keV  $2^+$  level. All these facts support the proposed identification of the  $1^+$ ,  $2^+$ , and  $3^+$  members of the  $\pi d5/2\nu\bar{d}3/2$  multiplet. We remark that the 541 keV  $(3^+) \rightarrow 82$  keV  $(4^+)$  transition has not been found in this study, and so we identify the  $4^+$  member with the 82-keV  $(4^+)$  state only tentatively.

**The  $\pi g7/2\nu\bar{s}1/2$  doublet.** On the basis of the level-energy systematics of the  $\pi g7/2\nu\bar{s}1/2$  doublet in  $^{116,120,122,124}\text{Sb}$ , we may expect the  $^{118}\text{Sb}$   $3^+$  and  $4^+$  members of this doublet in the 300–600-keV region. The parabolic rule predicts that  $E_{\text{lev}}(3^+) < E_{\text{lev}}(4^+)$ . Candidates for the  $3^+$  and  $4^+$  members of this doublet may be the 403.5-keV  $(3^+)$  and 557-keV  $(4^+, 3^+)$  states, respectively, which are connected by a strong transition.

**The  $\pi d5/2\nu\bar{g}7/2$  multiplet.** The calculations predict a positive concave parabolic shape for the energy splitting of this multiplet, in a similar way as in  $^{116}\text{Sb}$  [33]. Owing to the uncertainty in spin-parity determinations, it is difficult to give an unambiguous identification of the

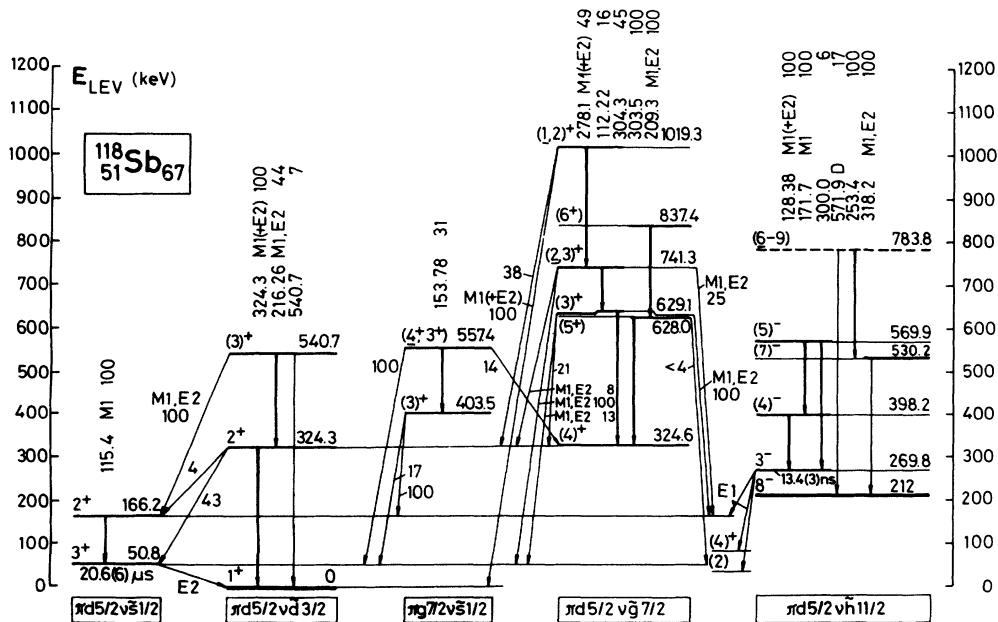


FIG. 12. Experimental decay properties of some low-lying levels of  $^{118}\text{Sb}$ . Approximate classification of the states according to different proton-neutron multiplets.

members of this multiplet. On the basis of the decay properties of levels (Fig. 12), the 1019-keV  $(1,2)^+$ , 741-keV  $(2,3)^+$ , 629-keV  $(3)^+$ , 324.6-keV  $(4)^+$ , 628-keV  $(5)^+$ , and 837-keV  $(6)^+$  states may correspond to the  $1^+$ ,  $2^+$ ,  $3^+$ ,  $4^+$ ,  $5^+$ , and  $6^+$  members of this multiplet, respectively.

*The  $\pi d5/2\nu\tilde{h}11/2$  multiplet.* The magnetic-moment measurements of Callaghan, Scott, and Stone [9] and Dima *et al.* [10] established a pure  $\pi d5/2\nu\tilde{h}11/2$  configuration for the 212-keV  $8^-$  and 270-keV  $3^-$  states. The calculations predict a negative concave parabolic shape for the energy splitting of this multiplet (Fig. 11). Some members of this multiplet have been observed in the neighboring  $^{116}\text{Sb}$  [33] and  $^{120}\text{Sb}$  [34] nuclei. Taking into account also the decay properties of the levels (Fig. 12), it is very likely that the  $3^-$ ,  $4^-$ ,  $5^-$ ,  $7^-$ , and  $8^-$  members of this multiplet are the 270-keV  $3^-$ , 398-keV  $(4)^-$ , 570-keV  $(5)^-$ , 530-keV  $(7)^-$ , and 212-keV  $8^-$  states, respectively. On the basis of the decay properties, the 784-keV  $(6-9)$  state may correspond to the  $6^-$  member of this multiplet, but owing to the uncertainty in spin determination and unknown parity, this assignment is only tentative.

*The  $\pi g7/2\nu\tilde{d}3/2$  and  $\pi g7/2\nu\tilde{h}11/2$  multiplets.* The calculations predict negative concave parabolic energy splitting for both multiplets. Although there are some candidates for the different members of these multiplets (Fig. 11), for reliable identification further experimental information is needed.

## VII. IBFFM CALCULATIONS, DISCUSSION

In order to get a deeper insight into the structure of the low-lying  $^{118}\text{Sb}$  states, we have calculated the energies and electromagnetic properties of the states on the basis of the interacting boson-fermion-fermion model.

The *Hamiltonian* of the interacting boson-fermion-fermion model [35] is

$$H_{\text{IBFFM}} = H_{\text{IBFM}}(p) + H_{\text{IBFM}}(n) - H_{\text{IBM}} + H_{pn},$$

where  $H_{\text{IBFM}}(p)$  and  $H_{\text{IBFM}}(n)$  are the IBFM Hamiltonians for the neighboring odd-even nuclei with an odd proton and odd neutron, respectively [36].  $H_{\text{IBM}}$  denotes the IBM Hamiltonian [37] for the even-even core nucleus.  $H_{pn}$  is the Hamiltonian of the residual  $p$ - $n$  interaction.

The core Hamiltonian was approximated with its SU(5) limit, which is reasonable for spherical nuclei in the Sn-Sb region.

The residual proton-neutron interaction has the following form:

$$H_{pn} = 4\pi\delta(\mathbf{r}_p - \mathbf{r}_n)[v_D + v_S(\boldsymbol{\sigma}_p \cdot \boldsymbol{\sigma}_n)] + V_{\sigma\sigma}[\boldsymbol{\sigma}_p \cdot \boldsymbol{\sigma}_n]_0.$$

This includes a spin-dependent delta interaction with an additional spin polarization term.

We have performed the calculations on the basis of the truncated quadrupole phonon model for odd-odd nuclei (OTQM), which is equivalent to the interacting boson-fermion-fermion model (IBFFM) on phenomenological level.

The IBFFM-OTQM Hamiltonian was diagonalized in the proton-neutron-boson basis:  $|(j_p, j_n)I, NR; J\rangle$ , where

$j_p$  and  $j_n$  stand for the proton and neutron angular momenta coupled to  $I$ ,  $N$  is the number of  $d$  bosons,  $R$  is their total angular momentum, and  $J$  is the spin of the state. The IBM/TQM, IBFM/PTQM, and IBFFM/OTQM computer codes, used in the calculations, were written by Brant, Paar, and Vretenar [38].

*Parametrization.* We have considered a maximum of two  $d$  bosons which is an acceptable approximation if we want to describe only the low-lying states of a nearly spherical nucleus. It is known that restriction of the boson number in the presence of SU(5) core can be accounted for by a renormalization of the parameters. The calculations showed that even the two-boson components were weak in the low-lying states (see Table VI). The boson-boson interaction was also omitted.

The shell-model space consisted of the  $2d5/2$ ,  $1g7/2$ ,  $3s1/2$ ,  $2d3/2$ , and  $1h11/2$  subshells for the proton particle and neutron quasiparticles.

The  $d$ -boson (quadrupole phonon) energy was the energy of the  $2_1^+$  state of the  $^{116}\text{Sn}$  core nucleus:  $\hbar\omega_2 = 1.29$  MeV.

The occupation probabilities for neutrons were taken from the systematics of available data (citations in Ref. [32]):  $V^2(vd5/2) = 0.88$ ,  $V^2(vg7/2) = 0.85$ ,  $V^2(vs1/2) = 0.51$ ,  $V^2(vd3/2) = 0.30$ , and  $V^2(vh11/2) = 0.23$ . In the parabolic rule calculation, we have used the same values.

The single-proton and quasineutron energies, as well as the dynamical ( $\Gamma_0$ ), exchange ( $\Lambda_0$ ), and monopole ( $A_0$ ) strength parameters of nucleon-core interaction, were fitted first to the energy spectra and known electromagnetic moments of  $^{117}\text{Sb}$  and  $^{117}\text{Sn}$  nuclei by IBFM calculations; later, they were slightly adjusted to the energy spectrum and electromagnetic moments of  $^{118}\text{Sb}$ . The best parameters were as follows. Single-proton energies:  $\epsilon(\pi d5/2) = 0$ ,  $\epsilon(\pi g7/2) = 0.33$ ,  $\epsilon(\pi s1/2) = 1.5$ ,  $\epsilon(\pi d3/2) = 1.2$ , and  $\epsilon(\pi h11/2) = 1.38$  (all in MeV); quasineutron energies:  $E(vd5/2) = 1.2$ ,  $E(vg7/2) = 0.5$ ,  $E(vs1/2) = 0$ ,  $E(vd3/2) = 0.44$ , and  $E(vh11/2) = 0.51$  (all in MeV); strength parameters:  $\Gamma_0^p = 0.65$ ,  $\Lambda_0^p = 0$ ,  $A_0^p = 0.08$ ,  $\Gamma_0^n = 0.6$ ,  $\Lambda_0^n = 1.3$ , and  $A_0^n = 0.1$  (all in MeV).

The  $V^2$  values and single-proton and quasineutron energies, as well as the strength parameters, showed a smooth variation in our IBFFM calculations for  $^{116}\text{Sb}$  [33],  $^{118}\text{Sb}$ , and  $^{120}\text{Sb}$  [34].

The parameters of the residual  $p$ - $n$  interaction were fitted to the energy spectrum and electromagnetic moments of  $^{118}\text{Sb}$ :  $v_D = -1.1$ ,  $v_S = -0.27$ , and  $V_{\sigma\sigma} = 0.09$  (all in MeV).

The effective charges and gyromagnetic ratios were close to the standard values:  $e^p = 1.5e$ ,  $e^n = 0.5e$ ,  $e^{\text{vib}} = 2.7e$ ,  $g_l^p = 1$ ,  $g_s^p = 0.65g_s^p(\text{free})$ ,  $g_l^n = 0$ ,  $g_s^n = 0.6g_s^n(\text{free})$ , and  $g_R = Z/A = 0.432$ .

The experimental and theoretical *level energies* of the low-lying states of  $^{118}\text{Sb}$  are shown in Fig. 13.

The *wave functions* of some low-lying states are shown in Table VI. The IBFFM calculations proved the approximate classification of the parabolic rule: The  $1_1^+$ ,  $2_2^+$ ,  $3_3^+$ , and  $4_1^+$  states are dominated with  $\pi d5/2\nu\tilde{d}3/2$ , the  $2_1^+$  and  $3_1^+$  states with  $\pi d5/2\nu\tilde{s}1/2$ , the  $3_2^+$  and  $4_3^+$  states with  $\pi g7/2\nu\tilde{s}1/2$ , the  $1_6^+$ ,  $2_3^+$ ,  $3_4^+$ ,  $4_2^+$ ,  $5_1^+$ , and  $6_1^+$

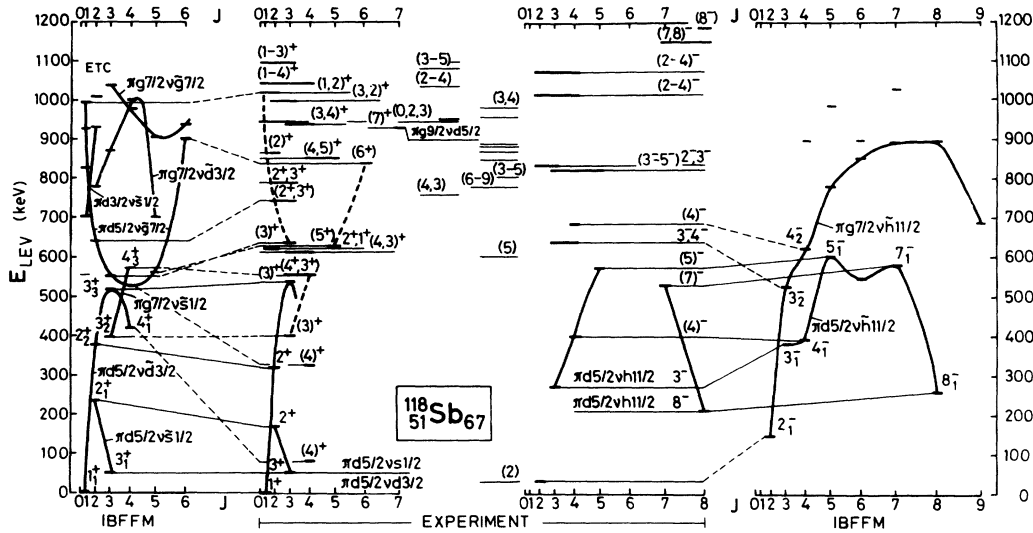


FIG. 13. Experimental and IBFFM theoretical energy spectra of  $^{118}\text{Sb}$  separately for positive- and negative-parity states. Thick solid lines connect levels having the same dominating configuration. The abscissa is scaled according to  $J(J + 1)$ , where  $J$  is the spin of the state.

states with  $\pi d5/2v\bar{g}7/2$ , the  $3_1^-, 4_1^-, 5_1^-, 6_1^-, 7_1^-$ , and  $8_1^-$  states with  $\pi d5/2v\bar{h}11/2$ , the  $2_1^-, 3_2^-, 4_2^-, 5_2^-, 6_2^-, 7_2^-$ ,  $8_2^-$ , and  $9_1^-$  states with  $\pi g7/2v\bar{h}11/2$  components, etc.

The magnetic dipole and electric quadrupole moments of the low-lying  $^{118}\text{Sb}$  states are given in Table VII. The IBFFM calculations give the signs of the moments, while from experiment only the absolute values of the moments could be determined in four cases. The numerical values

of the theoretical moments agree with the experimental ones within less than 10%.

The  $E2/M1$  mixing ( $\delta$ ) and  $\gamma$ -branching ratios of some low-lying states in  $^{118}\text{Sb}$  are given in Table VIII. The experimental branching ratios are reproduced within a factor of 10. The theoretical  $E2/M1$  mixing ratios agree with the experimental ones within experimental errors. The experimental half-life of the 51-keV isomeric level is

TABLE VI. Wave functions of some low-lying states of  $^{118}\text{Sb}$ . Only components with > 10% weight are given.

$J^\pi$	$(j_p, j_n)$	$I;NR$	Amplitude	$J^\pi$	$(j_p, j_n)$	$I;NR$	Amplitude
$1_1^+$	$(\frac{5}{2}, \frac{3}{2})$	1;00	0.863	$2_1^-$	$(\frac{7}{2}, \frac{11}{2})$	2;00	0.861
$2_1^+$	$(\frac{5}{2}, \frac{1}{2})$	2;00	-0.810	$3_1^-$	$(\frac{5}{2}, \frac{11}{2})$	3;00	0.777
$2_2^+$	$(\frac{5}{2}, \frac{3}{2})$	2;00	-0.821	$3_2^-$	$(\frac{7}{2}, \frac{11}{2})$	3;00	-0.721
	$(\frac{5}{2}, \frac{3}{2})$	1;12	0.363		$(\frac{7}{2}, \frac{11}{2})$	2;12	-0.363
$3_1^+$	$(\frac{5}{2}, \frac{1}{2})$	3;00	-0.891	$4_1^-$	$(\frac{5}{2}, \frac{11}{2})$	4;00	0.742
$3_2^+$	$(\frac{7}{2}, \frac{1}{2})$	3;00	0.846	$4_2^-$	$(\frac{7}{2}, \frac{11}{2})$	4;00	-0.716
	$(\frac{7}{2}, \frac{1}{2})$	3;12	-0.317		$(\frac{7}{2}, \frac{11}{2})$	2;12	0.482
$3_3^+$	$(\frac{5}{2}, \frac{3}{2})$	3;00	-0.585	$5_1^-$	$(\frac{5}{2}, \frac{11}{2})$	5;00	-0.798
	$(\frac{5}{2}, \frac{7}{2})$	3;00	-0.577		$(\frac{5}{2}, \frac{11}{2})$	7;12	0.337
$4_1^+$	$(\frac{5}{2}, \frac{3}{2})$	4;00	0.805	$8_1^-$	$(\frac{5}{2}, \frac{11}{2})$	8;00	0.844
	$(\frac{5}{2}, \frac{3}{2})$	4;12	-0.376		$(\frac{5}{2}, \frac{11}{2})$	8;12	-0.431
$4_2^+$	$(\frac{5}{2}, \frac{7}{2})$	4;00	0.574				
	$(\frac{7}{2}, \frac{1}{2})$	4;00	0.548				
$4_3^+$	$(\frac{7}{2}, \frac{1}{2})$	4;00	-0.651				
	$(\frac{5}{2}, \frac{7}{2})$	4;00	0.511				
$5_1^+$	$(\frac{5}{2}, \frac{7}{2})$	5;00	-0.851				
	$(\frac{5}{2}, \frac{7}{2})$	6;12	-0.319				
$6_1^+$	$(\frac{5}{2}, \frac{7}{2})$	6;00	0.828				
	$(\frac{5}{2}, \frac{7}{2})$	5;12	-0.468				

TABLE VII. Magnetic dipole ( $\mu$  in  $\mu_N$ ) and electric quadrupole ( $Q$  in  $e b$ ) moments of the low-lying  $^{118}\text{Sb}$  states.

$J^\pi$ (state)	main configuration	$\mu$		$Q$	
		Expt.	IBFFM	Expt.	IBFFM
$1_1^+$ (ground)	$\pi d5/2\nu d3/2$	$\pm 2.46(7)$ [6]	+2.31		-0.14
$3_1^+$ (51 keV)	$\pi d5/2\nu s1/2$	$\pm 2.61(5)$ [7]	+2.58	$\pm 0.57(14)^a$ [8]	-0.57
$8_1^-$ (212 keV)	$\pi d5/2\nu h11/2$	$\pm 2.32(4)$ [9]	+2.54		-0.92
$3_1^-$ (270 keV)	$\pi d5/2\nu h11/2$	-3.76(9) [10,12]	-3.43	$\pm 0.25(5)^a$ [10]	-0.26

<sup>a</sup>“Sternheimer” or other polarization correction included [12].

$T_{1/2} = 20.6 \pm 0.6 \mu\text{s}$  [7], while the IBFFM/OTQM calculations give  $2 \mu\text{s}$ .

### VIII. INTRUDER STATES IN $^{118}\text{Sb}$

It is known that systematic  $\Delta J = 1$  bands are built on low-lying  $\frac{9}{2}^+$  proton-hole (two-particle-one-hole) states in  $^{113,115,117,119,121,123}\text{Sb}$  nuclei [27]. The  $\frac{9}{2}^+$  states are fed by a bandlike cascade of  $J \rightarrow J-1$   $\gamma$ -ray transitions and with  $J \rightarrow J-2$  crossovers. The experimental level energies of the  $^{117}\text{Sb}$   $\pi g_{9/2}^{-1}$  intruder band are presented in Fig. 14; intruder bands of the other odd- $A$  Sb nuclei are very similar.

$\Delta J = 1$  collective bands have been observed also in  $^{114}\text{Sb}$ ,  $^{116}\text{Sb}$  [39,40], and  $^{118,120}\text{Sb}$  [4] nuclei based on  $8^-$  states. The level-spacing properties show strong resemblance with the bands observed in odd- $A$  nuclei. In the present work, the  $8^-$ ,  $9^-$ ,  $10^-$ , and  $11^-$  members of the band have been observed in  $^{118}\text{Sb}$  from the  $(\alpha, n\gamma)$  reaction. The results are presented on the right-hand side of Fig. 14, together with the data of Vajda *et al.* [4] on the  $12^-$  and  $13^-$  states.

In the framework of the IBF-PTQ model, we have calculated the energy levels of the intruder band of  $^{117}\text{Sb}$ . In these simple calculations, we have supposed that there is a proton hole in the  $^{118}\text{Te}$  core, and configuration mixing with other states has been neglected. A maximum of four

phonons have been taken into account, and the energy of the first  $2_1^+$  state of  $^{118}\text{Te}$  was used as  $d$ -boson (quadrupole phonon) energy:  $h_1 = \hbar\omega_2 = 0.6$  MeV. The IBFFM-PTQM results obtained at  $h_2 = -0.02$  MeV,  $h_3 = 0.2$  MeV,  $h_{40} = h_{42} = h_{44} = 0$ ,  $N_{\text{max}} = 4$ ,  $A_0^p = 0.03$  MeV,  $\Gamma_0^p = 0.65$  MeV, and  $\Lambda_0^p = 0$  MeV parameters are presented on the left-hand side of Fig. 14. The conclusion of this calculation is that the account of  $h_2$  and  $h_3$  anharmonicities is very important, which hints at the presence of  $\beta$  and  $\gamma$  deformation in these states. The meaning of the  $\{h\}$  parameters is explained in [36(b)].

According to our parabolic rule calculations, the splitting of the  $\pi g_{9/2}^{-1} \nu \tilde{h} 11/2$   $^{118}\text{Sb}$  multiplet shows a positive concave parabolic shape with a minimum energy at the  $8^-$  state. (The energies of the  $7^-$  and  $8^-$  states are very close to each other.)

In the framework of the IBFFM-OTQM, we have calculated the energy spectrum of the intruder band of  $^{118}\text{Sb}$ . The 1186-keV  $8^-$  state of the  $\pi g_{9/2}^{-1} \nu \tilde{h} 11/2$  multiplet was taken as the head of the band. Using the same  $h_1 = \hbar\omega_2 = 0.6$  MeV,  $h_2 = -0.02$  MeV,  $h_3 = 0.2$  MeV,  $h_{40} = h_{42} = h_{44} = 0$ ,  $\Gamma_0^p = 0.65$  MeV, and  $\Lambda_0^p = 0$  MeV parameters as in the case of  $^{117}\text{Sb}$ , as well as  $V^2(\nu \tilde{h} 11/2) = 0.27$ ,  $A_0^p = A_0^n = 0$ ,  $\Gamma_0^n = 0.7$  MeV,  $\Lambda_0^n = 1.3$  MeV,  $v_D = -1.3$  MeV,  $v_S = -0.2$  MeV,  $V_{\sigma\sigma} = 0.06$  MeV, and  $N_{\text{max}} = 3$  parameters, which are close to the parameters used for the description of the energy spectra of  $^{116}\text{Sb}$  [33],  $^{118}\text{Sb}$ , and  $^{120}\text{Sb}$  [34] nuclei, we have obtained

TABLE VIII. Transitions within some low-lying states of  $^{118}\text{Sb}$ .

$E_i$ (keV)	$J_i^\pi$	$E_f$ (keV)	$J_f^\pi$	Experimental data			IBFFM calc.		
				$E_\gamma$ (keV)	Multipolarity	$\delta$	$I_\gamma$	$ \delta $	$I_\gamma$
51	$3_1^+$	0	$1_1^+$	51	$E2$	pure $E2$	100	pure $E2$	100
166	$2_1^+$	51	$3_1^+$	115	$M1$	0.02(15)	100	0.02	100
324	$2_2^+$	166	$2_1^+$	158			4(2)	0.01	1.3
		51	$3_1^+$	274			43(5)	0.02	12
541	$(3)_3^+$	0	$1_1^+$	324	$M1(+E2)$	-0.09(17)	100	0.11	100
		324	$2_2^+$	216	$M1, E2$	0.06(7)	44(5)	0.04	113
		166	$2_1^+$	375	$M1, E2$	-0.06(5)	100	0.09	100
403	$(3)_2^+$	0	$1_1^+$	541			7(3)	pure $E2$	24
		166	$2_1^+$	237			100	0.43	100
		51	$3_1^+$	353			17(3)	2.11	19
570	$(5)_1^-$	398	$(4)_1^-$	172	$M1$		100	0.02	100
		270	$3_1^-$	300			6(1)	pure $E2$	1
530	$(7)_1^-$	212	$8_1^-$	318	$M1, E2$		100	0.05	100

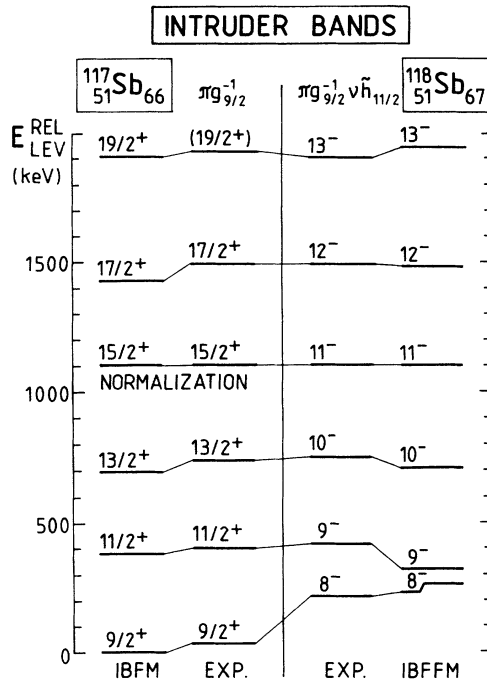


FIG. 14. Experimental and theoretical level energies of the intruder bands in  $^{117}\text{Sb}$  and  $^{118}\text{Sb}$ .

the results shown in Fig. 14 (subscript IBFFM). Aside from the low-energy part, where configuration mixing is expected with other  $8^-$ ,  $9^-$ , and  $10^-$  states, rather good agreement has been obtained between experiment and theory. The wave functions of the states contain different phonon components, and the dominating configurations

contain higher and higher phonon number components with increasing spin. The amplitudes squared for the band members as a function of the quadrupole phonon number were very similar to the results of Maldeghem, Sau, and Heyde [41], who have calculated the properties of the intruder band of  $^{116}\text{Sb}$  in a simplified odd-proton, odd-neutron vibrational core coupling model.

We remark that Nes *et al.* [40] explained the  $\Delta J = 1$  bands (in  $^{114,116}\text{Sb}$ ) in terms of rotational alignment of the  $h_{11/2}$  neutron with the deformed rotating odd- $A$  core. This model may give an alternative description of the  $\Delta J = 1$  band, but numerical results have not been published on  $^{118}\text{Sb}$ .

## IX. SUMMARY

In this work we have studied the structure of the  $^{118}\text{Sb}$  nucleus from the  $(p, n\gamma)$  and  $(\alpha, n\gamma)$  reactions with complex  $\gamma$  and electron spectroscopic methods. A new, more complete level scheme of  $^{118}\text{Sb}$  has been proposed with new spin-parity values. The parabolic rule calculation helped to identify several proton-neutron multiplet states. The IBFFM/OTQM calculations have given a reasonable description of the energy spectrum and electromagnetic properties of the low-lying  $^{118}\text{Sb}$  states.

## ACKNOWLEDGMENTS

We are indebted to Dr. Z. Gácsi, Dr. T. Kibédi, Dr. A. Krasznahorkay, Dr. S. Mészáros, A. Szücs, Dr. J. Timár, and Dr. A. Valek for their help in the measurements. This work was supported in part by the Hungarian Scientific Research Foundation (OTKA). We acknowledge also the financial support of the G. Soros Foundation.

- [1] W. B. Caffee, C. B. Morgan, R. A. Warner, W. C. McHarris, W. H. Kelly, E. M. Bernstein, and R. Shamu, Michigan State University, Cyclotron Laboratory, Annual Report, 1972, p. 32.
- [2] W. B. Chaffee, private communication, cited in G. H. Carlson, W. L. Talbert, Jr., and S. Raman, Nucl. Data Sheets **17**, 1 (1976); W. B. Chaffee, C. B. Morgan, J. Guile, R. A. Warner, L. E. Samuelson, W. H. Kelly, W. C. McHarris, E. M. Bernstein, and R. Shamu, Michigan State University, Cyclotron Laboratory, Annual Report, 1973, p. 52.
- [3] W. B. Chaffee, Ph.D. thesis, Michigan State University, 1983, pp. 1–189.
- [4] S. Vajda, W. F. Piel, Jr., M. A. Quader, W. A. Watson III, F. C. Yang, and D. B. Fossan, Phys. Rev. C **27**, 2995 (1983).
- [5] R. W. Fink, G. Andersson, and J. Kantele, Ark. Fys. **19**, 327 (1961); J. Hattula, E. Liukkonen, and J. Kantele, Z. Phys. **231**, 203 (1970).
- [6] A. D. Jackson, Jr., E. H. Rogers, Jr., and G. J. Garrett, Phys. Rev. **175**, 65 (1968).
- [7] D. Ploștinaru, E. A. Ivanov, G. Pascovici, and A. Iordăchescu, Phys. Lett. **57B**, 235 (1975).
- [8] F. Dimmling, Ph.D. thesis, Freie University, Berlin, 1977; H.-E. Mahnke, E. Dafni, M. H. Rafailovich, G. D. Sprouse, and E. Vapirev, Phys. Rev. C **26**, 493 (1982).
- [9] P. T. Callaghan, M. Shott, and N. J. Stone, Nucl. Phys. **A221**, 1 (1974).
- [10] S. Dima, M. Duma, M. Ionescu-Bujor, A. Iordăchescu, G. Pascovici, and C. Stan-Sion, Z. Phys. A **320**, 613 (1985).
- [11] M. Ionescu-Bujor, A. Iordăchescu, G. Pascovici, and V. Sabaiduc, Phys. Lett. B **200**, 259 (1988).
- [12] P. Raghavan, At. Data Nucl. Data Tables **42**, 189 (1989).
- [13] T. Tamura, K. Miyano, and S. Ohya, Nucl. Data Sheets **51**, 329 (1987).
- [14] A. H. Wapstra and G. Audi, Nucl. Phys. **A432**, 1 (1985); **A432**, 55 (1985).
- [15] Z. Árvay, T. Fényes, K. Füle, T. Kibédi, S. László, Z. Máté, Gy. Móri, D. Novák, and F. Tárkányi, Nucl. Instrum. Methods **178**, 85 (1980); T. Kibédi, Z. Gácsi, A. Krasznahorkay, and S. Nagy, ATOMKI, Debrecen, Annual Report, 1986, p. 55; T. Kibédi, Z. Gácsi, and A. Krasznahorkay, ATOMKI, Institute of Nuclear Research, Debrecen, Annual Report, 1987, p. 100.

- [16] H. Helppi, University of Jyväskylä, JYFL Report No. 1/1976, 1976.
- [17] E. Sheldon and V. C. Rogers, *Comput. Phys. Commun.* **6**, 99 (1973).
- [18] M. Jääskeläinen, University of Jyväskylä, JYFL Report No. 3/84, 1984.
- [19] G. Székely, *Comput. Phys. Commun.* **34**, 313 (1985).
- [20] F. Rösel, H. M. Fries, K. Alder, and H. C. Pauli, *At. Data Nucl. Data Tables* **21**, 91 (1978).
- [21] D. Wilmore and P. E. Hodgson, *Nucl. Phys.* **55**, 673 (1964).
- [22] M. Józsa, Z. Máté, T. Vertse, and Z. Zolnai, ATOMKI, Institute of Nuclear Research, Debrecen, Annual Report, 1989, p. 12.
- [23] T. Ishimatsu, K. Yagi, H. Ohmura, Y. Nakajima, T. Nakagawa, and H. Orihara, *Nucl. Phys.* **A104**, 481 (1967).
- [24] M. Conjeaud, S. Harar, and Y. Cassagnou, *Nucl. Phys.* **A117**, 449 (1968).
- [25] S. Gales, C. P. Massolo, S. Fortier, J. P. Schapira, P. Martin, and V. Compart, *Phys. Rev. C* **31**, 94 (1985).
- [26] P. Van Isacker, M. Waroquier, H. Vincx, and K. Hyde, *Nucl. Phys.* **A292**, 125 (1977).
- [27] R. E. Shroy, A. K. Gaigalas, G. Schatz, and D. B. Fossan, *Phys. Rev. C* **19**, 1324 (1979).
- [28] E. J. Schneid, A. Prakash, and B. L. Cohen, *Phys. Rev.* **156**, 1316 (1967).
- [29] P. L. Carson and L. C. McIntyre, Jr., *Nucl. Phys.* **A198**, 289 (1972).
- [30] P. H. Stelson, W. T. Milner, F. K. McGowan, R. L. Robinson, and S. Raman, *Nucl. Phys.* **A190**, 197 (1972).
- [31] V. Paar, *Nucl. Phys.* **A331**, 16 (1979).
- [32] T. Kibédi, Zs. Dombrádi, T. Fényes, A. Krasznahorkay, J. Timár, Z. Gácsi, A. Passoja, V. Paar, and D. Vretenar, *Phys. Rev. C* **37**, 2391 (1988).
- [33] Z. Gácsi, T. Fényes, and Zs. Dombrádi, *Phys. Rev. C* **44**, 626 (1991); Z. Gácsi, Zs. Dombrádi, T. Fényes, S. Brant, and V. Paar, *ibid.* **44**, 642 (1991).
- [34] T. Fényes and Zs. Dombrádi, *Phys. Lett. B* **275**, 7 (1992).
- [35] V. Paar, in *In-Beam Nuclear Spectroscopy*, edited by Zs. Dombrádi and T. Fényes (Akadémiai Kiadó, Budapest, 1984), Vol. 2, p. 675.
- [36] (a) F. Iachello and O. Scholten, *Phys. Rev. Lett.* **43**, 679 (1979); (b) V. Paar, S. Brant, L. F. Canto, G. Leander, and M. Vouk, *Nucl. Phys.* **A378**, 41 (1982).
- [37] D. Janssen, R. V. Jolos, and F. Dönau, *Nucl. Phys.* **A224**, 93 (1974); A. Arima and F. Iachello, *Phys. Rev. Lett.* **35**, 1069 (1975).
- [38] S. Brant, V. Paar, and D. Vretenar, computer codes IBM/TQM, IBFM/PTQM, and IBFFM/OTQM (Institut für Kernphysik, KFA, Jülich, 1985) (unpublished).
- [39] R. Duffait, J. Van Maldeghem, A. Charvet, J. Sau, K. Heyde, A. Emsalle, M. Meyer, R. Béraud, J. Thérèrne, and J. Genevey, *Z. Phys. A* **307**, 259 (1982).
- [40] P. Van Nes, W. H. A. Hesselink, W. H. Dickhoff, J. J. Van Ruyven, M. J. A. De Voigt, and H. Verheul, *Nucl. Phys.* **A379**, 35 (1982).
- [41] J. Van Maldeghem, J. Sau, and K. Heyde, *Phys. Lett.* **116B**, 387 (1982).